nature metabolism

Article

https://doi.org/10.1038/s42255-024-01114-8

Regulated and adaptive in vivo insulin secretion from islets only containing β-cells

Received: 26 April 2023

Accepted: 22 July 2024

Published online: 21 August 2024

Check for updates

Marta Perez-Frances[1], Eva Bru-Tari[1], Christian Cohrs[2,3], Maria Valentina Abate[1], Léon van Gurp[1], Kenichiro Furuyama[1,4], Stephan Speier[2,3], Fabrizio Thorel[1,5] & Pedro L. Herrera[1,5]

Insulin-producing β-cells in pancreatic islets are regulated by systemic cues and, locally, by adjacent islet hormone-producing 'non-β-cells' (namely α-cells, δ-cells and γ-cells). Yet whether the non-β-cells are required for accurate insulin secretion is unclear. Here, we studied mice in which adult islets are exclusively composed of β-cells and human pseudoislets containing only primary β-cells. Mice lacking non-β-cells had optimal blood glucose regulation, enhanced glucose tolerance, insulin sensitivity and restricted body weight gain under a high-fat diet. The insulin secretion dynamics in islets composed of only β-cells was comparable to that in intact islets. Similarly, human β-cell pseudoislets retained the glucose-regulated mitochondrial respiration, insulin secretion and exendin-4 responses of entire islets. The findings indicate that non-β-cells are dispensable for blood glucose homeostasis and β-cell function. These results support efforts aimed at developing diabetes treatments by generating β-like clusters devoid of non-β-cells, such as from pluripotent stem cells differentiated in vitro or by reprograming non-β-cells into insulin producers in situ.

Glucose homeostasis is the maintenance of blood glucose (glycaemia) levels within a narrow range to meet the body's fluctuating metabolic demands. The rapid and delicate adjustment of glycaemia involves a complex interplay of hormones and neuropeptides that are released into the blood from multiple organs, including the brain, liver, intestine, adipose tissue, muscle and pancreas.

Pancreatic islets have an essential role in glucose homeostasis through the secretion of various hormones, particularly insulin, which stimulates blood glucose uptake from peripheral tissues. Insulin released from β-cells is tightly regulated by circulating glucose levels but also by stimuli originating from islet α-cells, δ-cells and γ-cells[1]. For example, glucagon (GCG) produced by α-cells is a major glucose counter-regulatory hormone through its actions in modulating β-cell secretory activity[2]. Indeed, blocking GCG signalling by inactivating the GCG receptor (GCGR) or using GCGR-neutralizing antibodies reduces insulin release[2,3]. Moreover, corticotropin-releasing hormone and acetylcholine, both secreted from α-cells, can stimulate insulin secretion under certain physiological conditions[4,5]. Glucose-induced somatostatin (SST) secretion by δ-cells is also a powerful inhibitor of both GCG and insulin secretion[6]. Lastly, the pancreatic polypeptide (PPY) secreted from γ-cells can also reduce the secretion of insulin[7,8]. Collectively, these results strongly suggest that neighboring islet α-cells, δ-cells and- γ-cells have an important role in controlling insulin secretion from β-cells.

We have previously shown that islet non-β-cells have the intrinsic capacity of being converted to insulin-producing β-like cells under certain conditions, such as, for example, upon the loss of β-cells, which is a feature of diabetes mellitus[9–14]. Observing such plasticity in endogenous islet α-cells, δ-cells and γ-cells raises the possibility of exploiting this property to treat diabetes. This therapeutic strategy will result in

[1]Department of Genetic Medicine and Development, iGE3 and Centre facultaire du diabète, Faculty of Medicine, University of Geneva, Geneva, Switzerland. [2]Institute of Physiology, Faculty of Medicine, Technische Universität Dresden, Dresden, Germany. [3]Paul Langerhans Institute Dresden of the Helmholtz Zentrum München at the University Clinic Carl Gustav Carus of Technische Universität Dresden, Helmholtz Zentrum München, Neuherberg, Germany. [4]Present address: Center for iPS Cell Research and Application (CiRA), Kyoto University, Kyoto, Japan. [5]These authors contributed equally: Fabrizio Thorel, Pedro L. Herrera. e-mail: pedro.herrera@unige.ch

islets that exclusively contain surrogate insulin-producing cells, and it is unknown whether interfering with local intra-islet signalling will impact insulin secretion and blood glucose homeostasis in vivo. Consequently, we developed a mouse model that selectively and simultaneously removed α-cells, δ-cells and γ-cells while preserving an intact β-cell mass. In addition, we studied monotypic pseudoislets containing human primary β-cells only. These approaches enabled the exploration of how regulated insulin secretion and blood glucose homeostasis are affected in islets composed exclusively of β-cells.

Results

Generation of a mouse model of islet non-β-cell loss

To determine the necessity of islet non-β-cells in controlling glucose homeostasis and β-cell function, we generated triply transgenic mice allowing the inducible diphtheria toxin (DT)-mediated ablation of adult α-cells, δ-cells and γ-cells ('non-βDTR' mice). DT receptor (DTR) expression in islet cells was driven by the *Gcg*, *Sst* and *Ppy* promoters. The non-βDTR mice were obtained by breeding the Glu-DTR (transgenic)[15] and Ppy-DTR (knock-in)[14] lines to a new Sst-DTR knock-in line. Sst-DTR mice were generated using CRISPR technology to replace the coding sequence of the *Sst* gene with the DTR coding region (Fig. 1a). The knock-in Sst-DTR and Ppy-DTR alleles were bred to hemizygosity in non-βDTR mice (Fig. 1b) to secure both hormone and DTR expression in δ-cells and γ-cells, respectively (Fig. 1c).

Non-βDTR mice were given DT at 2 months of age. DT-treated non-βDTR mice (hereafter, 'β-only' mice) showed a >99% reduction in α-cell, δ-cell and γ-cell numbers 4 weeks post ablation (wpa; that is, at 3 months of age) compared with untreated mice (GCG^+ > 99.9%, SST^+ > 99.9%, PPY^+ > 99.9% ablation efficiency; Fig. 1d,e). Islet *Gcg*, *Sst* and *Ppy* mRNA levels were reduced to 0.4%, 0.2% and 0.5%, respectively (Fig. 1f). The near total loss of α-cells, δ-cells and γ-cells was maintained in mice approaching 1 year of age (40 wpa), with no evidence of non-β-cell regeneration (Fig. 1d,e and Extended Data Fig. 1). Pancreatic insulin content was unaltered in β-only mice (Fig. 1g and Extended Data Fig. 1). In conclusion, the non-βDTR line allows the selective, inducible and efficient ablation of α-cells, δ-cells and γ-cells and thus represents a unique model to study the regulatory properties of pancreatic islets composed exclusively of β-cells.

Proper glucose homeostasis in β-only mice

To examine the effect of non-β-cell loss on blood glucose regulation, male and female β-only mice were analysed longitudinally for a period of 40 wpa. These mice were healthy, with normal glycaemia, body weight and body composition (Fig. 2a and Extended Data Figs. 2 and 3). Yet there was a transient reduction in glycaemia and body weight at 2 wpa, coincident with the DT-mediated ablation of gut SST-expressing δ-cells (Extended Data Figs. 2 and 3). However, intestinal δ-cells were restored and SST circulating levels were back to normal by 30 days post ablation (dpa) (Extended Data Fig. 2). Of note, this transient drop in glycaemia and body weight was also observed after the ablation of δ-cells only, but not after the loss of either α-cells or γ-cells separately (Extended Data Fig. 4 and Supplementary Table 1). To avoid any confounding effects caused by this transient phenotype, all subsequent experiments were performed using β-only mice at 4 wpa or later time points.

Hypothalamic *Sst*-expressing neurons probably exert an orexigenic function by controlling feeding and physical behaviours[16–19]. After DT treatment, the ablation of SST^+ neurons was only partial in β-only mice, which may explain the unaltered food intake and locomotor activity (Extended Data Fig. 2). β-only mice were normoglycaemic under random-fed conditions and after short and prolonged fasting despite the drastic reduction in pancreatic GCG (Figs. 2a and 3a). Indeed, the moderate decrease in circulating GCG, which was already reported after α-cell ablation[15,20], as well as the normal levels of plasma counter-regulatory hormones (cortisol, growth hormone and epinephrine) probably prevented hypoglycaemia (Fig. 3b–f)[3,21]. In addition, liver-induced glucose mobilization, pyruvate and lactate levels, glycogen storage as well as the mRNA levels of gluconeogenic enzymes were comparably regulated in β-only and controls (that is, untreated non-βDTR mice) after a prolonged 16-h fasting challenge (Fig. 3g–k). These observations support previous reports indicating that the counter-regulatory responses to hypoglycaemia are maintained after extreme α-cell loss[3].

We then assessed glucose tolerance in β-only males and females. Oral, but not intraperitoneal glucose tolerance was improved after DT treatment, suggesting that non-β-cell ablation leads to an enhanced incretin effect (Fig. 2b–d and Extended Data Fig. 3). Notably, circulating GLP-1 levels and glucose-stimulated insulin secretion were increased in β-only mice after glucose gavage (Fig. 2e,f and Extended Data Fig. 3). DT-treated mice also exhibited improved insulin sensitivity correlating with increased glucose uptake in white adipose tissue (WAT; Fig. 2g,h and Extended Data Fig. 3). Enhanced insulin sensitivity was further confirmed with a hyperinsulinemic–euglycaemic clamp: β-only mice showed increased glucose infusion rate, enhanced hepatic insulin sensitivity and higher glucose absorption in WAT (Extended Data Fig. 5). Metabolic cages were then used to further characterize the metabolic status of β-only mice. Although energy expenditure was similar during the dark phase, a slight increase during the light period was observed in DT-treated mice (Fig. 2i). Interestingly, the subtle but significant decrease in the respiratory exchange ratio during the day phase indicated that β-only mice rely more on lipid than carbohydrate catabolism (Fig. 2j). The observed increase in glucose uptake in WAT, together with the higher lipid catabolism, suggests that adipose tissue metabolism is enhanced in β-only mice. Altogether, these results revealed that the absence of α-cells, δ-cells and γ-cells does not lead to detrimental effects on glucose homeostasis. Instead, several metabolic parameters are improved.

Improved glucose homeostasis in β-only mice on a high-fat diet

As the ablation of islet non-β-cells had no deleterious effects on glucose regulation under homeostatic conditions, we next investigated how the metabolic stress induced by a high-fat diet (HFD) affects β-only mice relative to controls. To this end, we devised four experimental groups of mice treated with or without DT and raised on either a chow or HFD (60% fat) regimen. High-fat or control diets were given to 3-month-old males (4 wpa) for 24 weeks (Fig. 4a). Strikingly, DT-treated non-βDTR animals showed a restricted body weight gain and limited increase in fat mass under HFD compared to challenged control mice (Fig. 4b,c). Importantly, food intake quantities were equal in all experimental groups (Extended Data Fig. 6). Fasting and random-fed glycaemia in the HFD group were higher in mice with intact islets relative to β-only animals (Fig. 4d and Extended Data Fig. 6). In addition, β-only mice exhibited better glucose tolerance than controls, which became glucose-intolerant (Fig. 4e and Extended Data Fig. 6). Of note, oral glucose tolerance in β-only mice under a HFD was like that of control mice under a chow diet (Fig. 4e). The control mice also manifested higher basal and glucose-stimulated insulin secretion than β-only mice under the HFD regimen. This suggests that HFD treatment triggers insulin resistance in control but not in β-only mice (Fig. 4f and Extended Data Fig. 6). This was confirmed by the worsened insulin sensitivity in HFD-raised control mice (Fig. 4g). By contrast, β-only mice challenged with HFD retained the improved insulin sensitivity first observed under homeostatic conditions (Fig. 4g). Thus, the combined loss of GCG-expressing, SST-expressing and PPY-expressing cells limits body weight gain rates under HFD. This can be explained, at least in part, by the enhanced insulin sensitivity acquired after non-β-cell ablation.

Islet non-β-cell loss drives the phenotype of β-only mice

The significant decrease in the number of SST-expressing neurons in the brain upon DT-mediated non-β-cell ablation (Extended Data Fig. 2)

https://doi.org/10.1038/s42255-024-01114-8

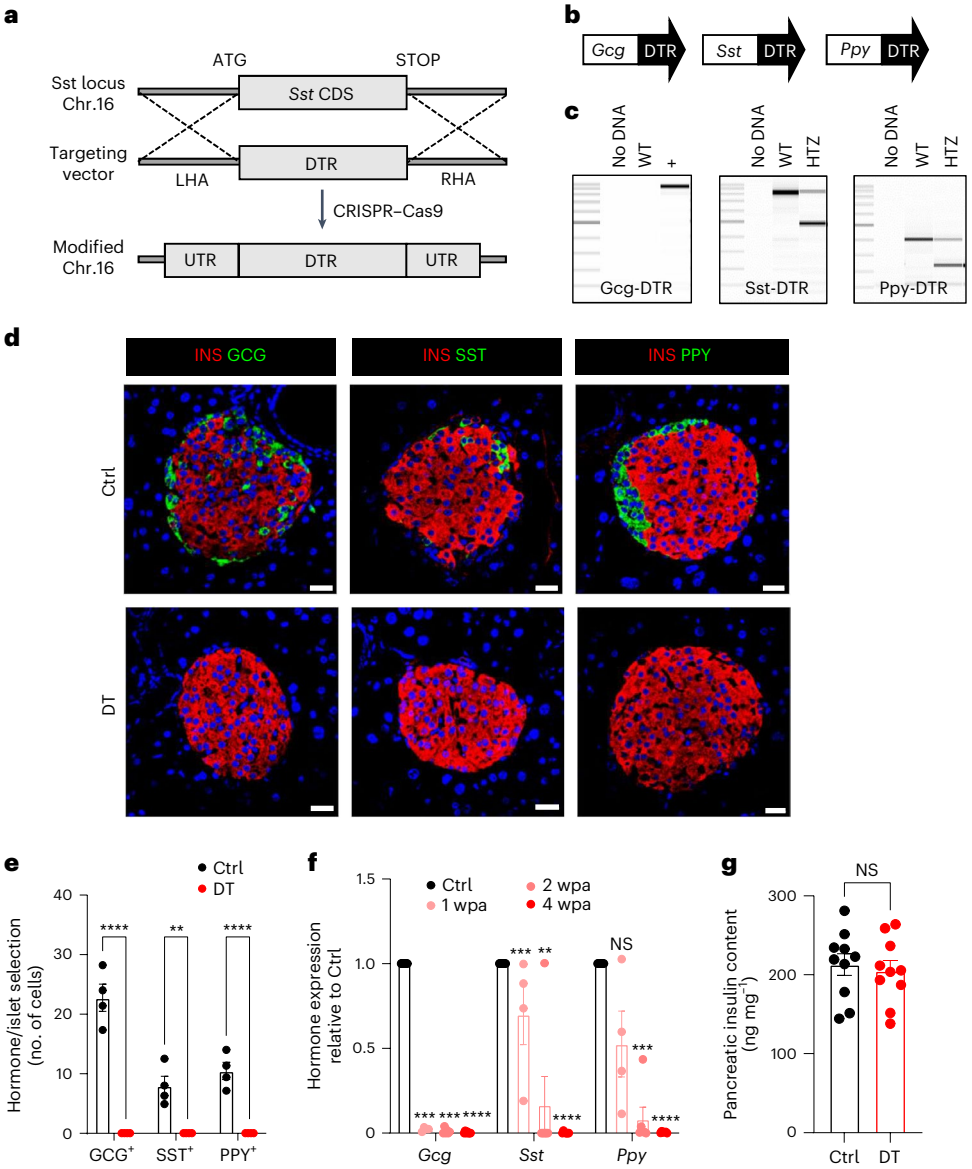

Fig. 1 | Generation and characterization of transgenic mice for the simultaneous ablation of islet α-cells, δ-cells and γ-cells. a, CRISPR–Cas9 strategy to replace the *Sst* coding sequence (*Sst* CDS) on mouse chromosome 16 with the human *DTR* coding region (targeting vector). LHA, left homology arm; RHA, right homology arm; UTR, untranslated region. **b**, Transgenes required for DTR-mediated non-β-cell ablation. **c**, PCR products of Gcg-DTR (~800 bp), Sst-DTR (WT 871 bp, KI 483 bp) and Ppy-DTR (WT 389 bp, KI 223 bp) transgenes. WT, wild type; HTZ, heterozygous. 'No DNA' is a negative control. **d**, Immunofluorescence on pancreatic sections from control (Ctrl) or β-only mice 4 wpa. INS, insulin (red); GCG, green (left); SST, green (middle); PPY, green (right). Scale bars, 20 µm. **e**, Quantification of GCG$^+$, SST$^+$ and PPY$^+$ cells in Ctrl ($n = 4$) or DT ($n = 5$) mice. GCG$^+$ and SST$^+$ cells were scored in the dorsal pancreas; PPY$^+$ cells were scored in the ventral pancreas. Statistical tests: two-way ANOVA. *P* values for Ctrl vs DT: GCG$^+$, $^{****}P < 0.0001$; SST$^+$, $^{**}P = 0.0012$; PPY$^+$, $^{****}P < 0.0001$. **f**, qPCR of *Gcg*, *Sst* and *Ppy* on isolated islets of Ctrl ($n = 10$) and β-only mice at 1 wpa ($n = 4$), 2 wpa ($n = 8$) and 4 wpa ($n = 7$). Data are normalized to housekeeping genes (*Gapdh* and *β-actin*) and shown as relative hormone expression to Ctrl. *P* values for *Gcg*: 1 wpa vs 0 wpa, $^{***}P = 0.0001$; 2 wpa vs 0 wpa, $^{***}P = 0.0001$; 4 wpa vs 0 wpa, $^{****}P = 0.00005$; *Sst*: 1 wpa vs 0 wpa, $^{***}P = 0.0001$; 2 wpa vs 0 wpa, $^{**}P = 0.007$; 4 wpa vs 0 wpa, $^{****}P = 0.00005$; *Ppy*: 1 wpa vs 0 wpa, $P = 0.056$; 2 wpa vs 0 wpa, $^{***}P = 0.0001$; 4 wpa vs 0 wpa, $^{****}P = 0.00005$. NS, not significant. **g**, Pancreatic insulin content of Ctrl ($n = 10$) and DT ($n = 10$) at 4 wpa. *P* value Ctrl vs DT, $P = 0.63$. All data are shown as mean ± s.e.m. Male and female mice were used for these experiments. Unless otherwise indicated, *P* values are from two-tailed Mann–Whitney tests. NS, not significant.

could impact the β-only phenotype in vivo. Yet lowering the DT dosage (three injections of 5 ng of DT) significantly spared SST$^+$ neurons without reducing the cell ablation efficiency in pancreatic islets (Extended Data Fig. 7). In the stomach, the SST-producing δ-cells were ablated at 15 dpa but reconstituted 2 weeks later, as in mice treated with the highest DT dose. Mice injected with 5 ng of DT did not display a sharp transient drop in body weight or glycaemia at 15 dpa (Extended Data Fig. 7), suggesting involvement of the SST-producing neurons in the transient phenotype observed with the high DT dosage. Interestingly, at 30 dpa, β-only mice treated with 5 ng of DT had improved oral glucose tolerance, glucose-stimulated insulin secretion and insulin sensitivity, similar to mice treated with a high DT dosage (Extended Data Fig. 7). Thus, the phenotype of β-only mice from 1 month post ablation is determined by the lack of islet non-β-cells.

β-only islets have a normal insulin secretion profile

To evaluate the intrinsic capacity of β-only islets to regulate insulin secretion without the influence of peripheral tissues, we assessed

https://doi.org/10.1038/s42255-024-01114-8

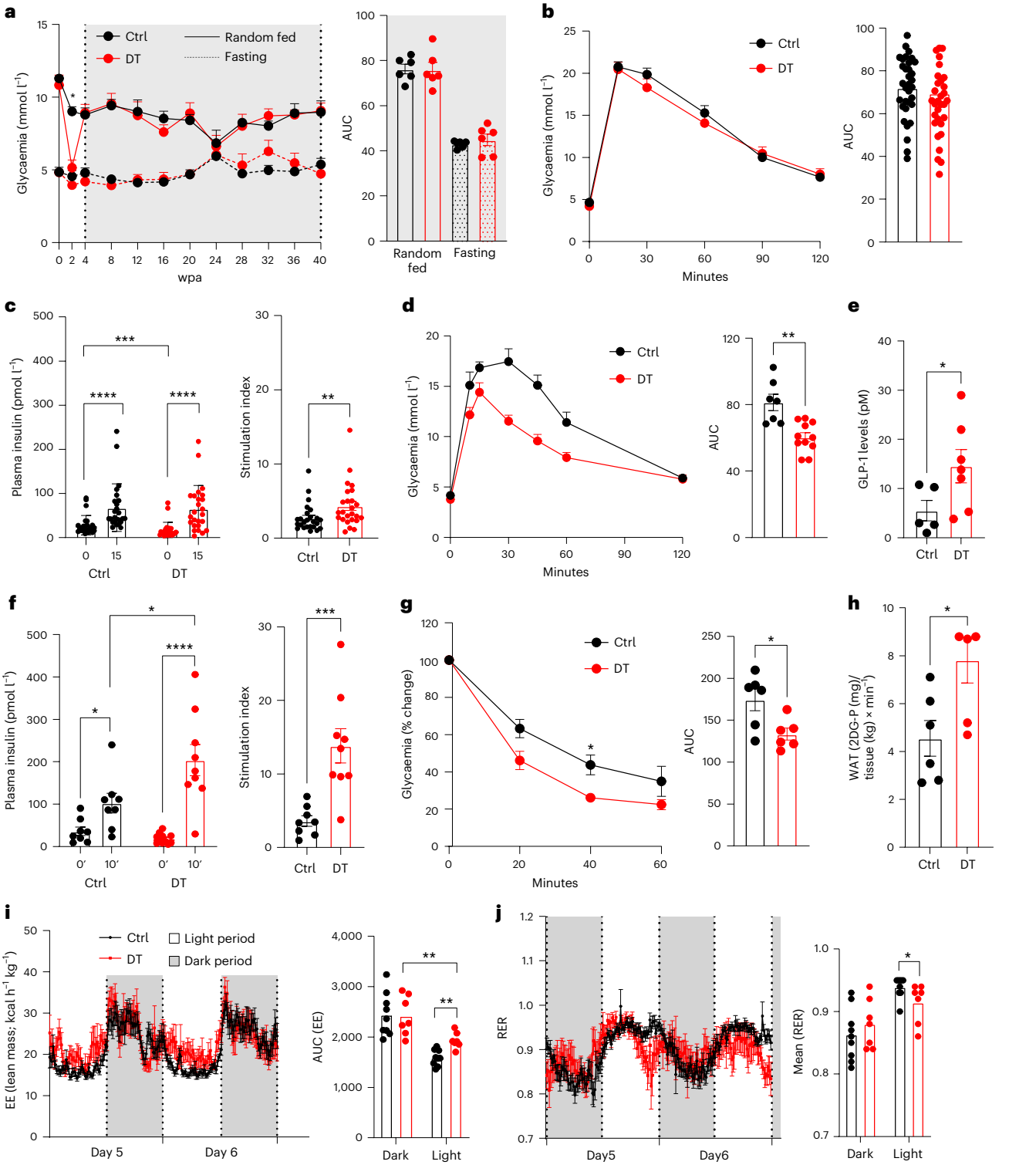

Fig. 2 | Optimal blood glucose homeostasis in mice whose islets comprise β-cells only. a, Glycaemia over 40 wpa in Ctrl ($n = 6$) and DT ($n = 6$) mice under random-fed (RF) or fasting (F) conditions. Right panel: area under the curve (AUC). *P* values (DT vs Ctrl): RF, $P = 0.73$; F, $P = 0.3939$. **b**, Intraperitoneal glucose tolerance test (ipGTT) on Ctrl ($n = 33$) and DT ($n = 34$). Right panel: AUC *P* value (Ctrl vs DT), $P = 0.3$. **c**, Plasma insulin 0 min and 15 min after glucose injection along ipGTT in Ctrl ($n = 25$) and DT ($n = 25$) mice. Right panel: stimulation index of insulin secretion. *P* value (Ctrl vs DT), $^{**}P = 0.0074$. **d**, Oral glucose tolerance test (oGTT) on Ctrl ($n = 7$) and DT ($n = 11$). Right panel: AUC *P* value (Ctrl vs DT), $^{**}P = 0.0028$. **e**, Plasma GLP-1 along oGTT in Ctrl ($n = 5$) and DT ($n = 7$) mice. *P* value (Ctrl vs DT), $^{*}P = 0.0303$. **f**, Plasma insulin 0 min and 10 min after glucose gavage along oGTT in Ctrl ($n = 8$) and DT ($n = 11$) mice. Right panel: stimulation index; *P* value (Ctrl vs DT), $^{***}P = 0.0006$. **g**, Insulin tolerance test (ITT) on Ctrl ($n = 6$) and DT ($n = 6$) mice. Data as % relative to glycaemia at time 0. Right panel: AUC of ITT; *P* value Ctrl vs DT, $^{*}P = 0.03$. **h**, Radiolabelled 2-deoxy-D-glucose (2DG) uptake by WAT in Ctrl ($n = 6$) and DT ($n = 6$) mice. *P* values (Ctrl vs DT), $^{*}P = 0.039$. **i**, Energy expenditure (EE) in Ctrl ($n = 9$) and DT ($n = 7$) mice. Right panel: AUC of EE, *P* value: light period Ctrl vs DT, $^{**}P = 0.0012$; Ctrl dark vs light period, $P < 0.0001$; DT dark vs light period, $^{**}P = 0.0047$. **j**, Respiratory exchange ratio (RER) in Ctrl (black, $n = 9$) and DT (red, $n = 7$) mice. Right panel: AUC of RER. *P* value: light period Ctrl vs DT, $^{*}P = 0.035$; Ctrl dark vs light period, $P < 0.0003$; DT dark vs light period, $P = 0.1212$. Only male mice were used. All data are shown as mean ± s.e.m.; *P* values are from two-tailed Mann–Whitney tests.

https://doi.org/10.1038/s42255-024-01114-8

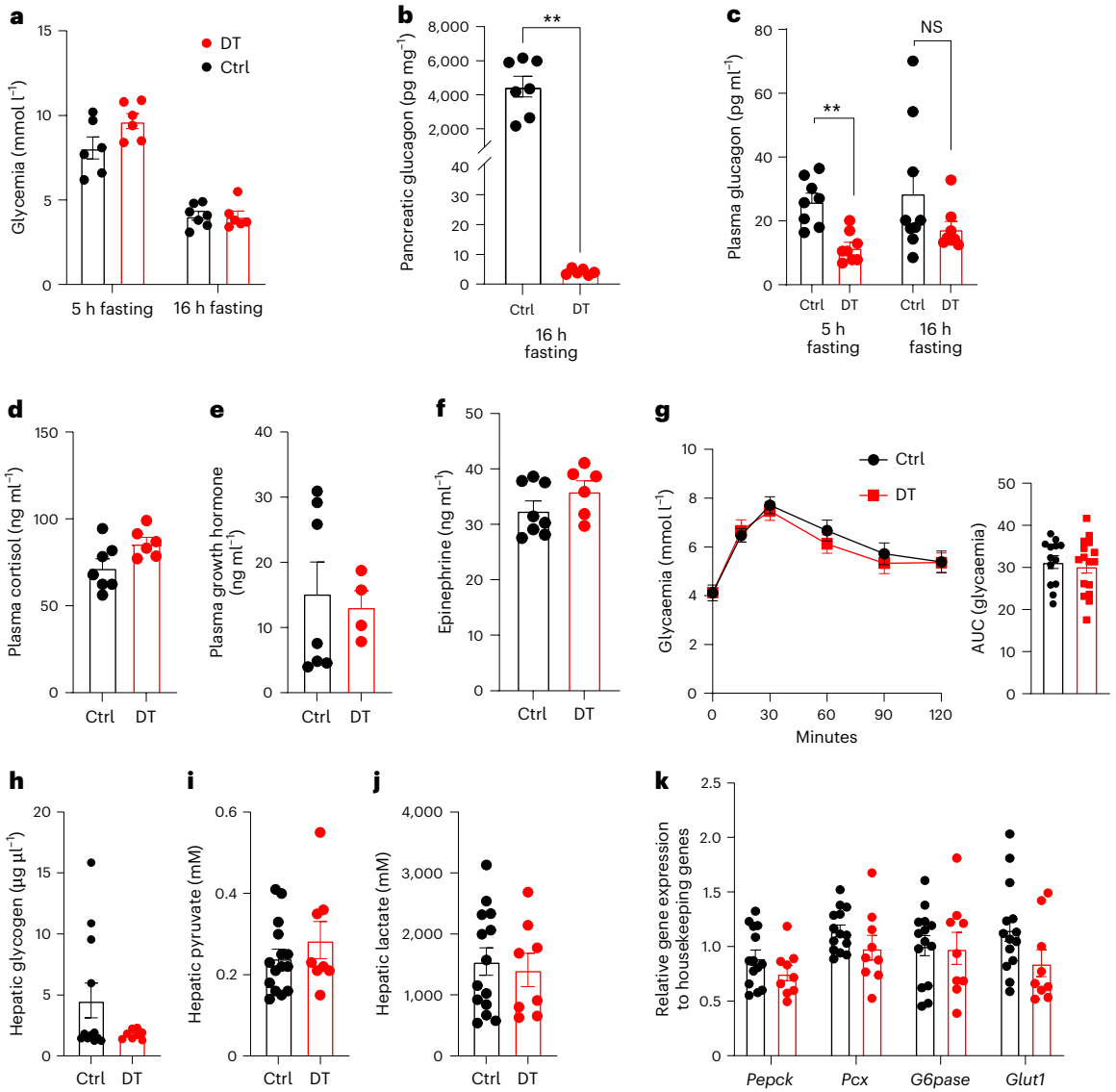

Fig. 3 | The ablation of pancreatic α-cells has no effect on GCG-mediated hepatic function. a, Glycaemia of control (Ctrl) and DT β-only mice after 5 h (Ctrl, $n = 6$; DT, $n = 6$) or 16 h (Ctrl, $n = 7$; DT, $n = 6$) fasting. P values (DT vs Ctrl): 5 h fasting, $P = 0.093$; 16 h fasting, $P = 0.7587$. **b**, Pancreatic GCG levels of Ctrl ($n = 7$) and DT ($n = 6$) β-only mice after 16 h fasting. P values: DT vs Ctrl, $^{**}P = 0.0012$. **c**, Plasma GCG levels of Ctrl and DT β-only mice after 5 h (Ctrl, $n = 8$; DT, $n = 8$) or 16 h (Ctrl, $n = 9$; DT, $n = 8$) fasting. P values: 5 h fasting DT vs Ctrl, $^{**}P = 0.0011$; 16 h fasting DT vs Ctrl, $P = 0.1447$. NS, not significant. **d**–**f**, Plasma cortisol (Ctrl $n = 7$; DT $n = 6$) (**d**), growth hormone (Ctrl $n = 7$; DT $n = 4$) (**e**) and epinephrine (Ctrl $n = 8$; DT $n = 6$) (**f**) levels of Ctrl and DT after 16 h fasting. P values DT vs Ctrl: cortisol, $P = 0.0688$; growth hormone, $P = 0.7879$; epinephrine, $P = 0.1074$. **g**, Pyruvate tolerance test (PTT) after 16 h fasting in Ctrl ($n = 13$) and DT ($n = 16$) mice. Right panel: AUC of PTT. P values: DT vs Ctrl, $P = 0.7136$. **h**–**j**, Hepatic glycogen (Ctrl $n = 12$; DT $n = 8$) (**h**), pyruvate (Ctrl $n = 15$; DT $n = 8$) (**i**) and lactate (Ctrl $n = 14$; DT $n = 8$) (**j**) levels after 16 h fasting in Ctrl and DT mice. P values DT vs Ctrl: glycogen, $P = 0.69$; pyruvate, $P = 0.579$; lactate, $P = 0.713$. **k**, Expression of hepatic gluconeogenic enzymes after 16 h fasting in Ctrl (black, $n = 14$) and DT (red, $n = 9$) mice. Phosphoenolpyruvate carboxykinase (*Pepck*), pyruvate carboxylase (*Pcx*), glucose-6-phosphatase (*G6pase*) and glucose transporter 1 (*Glut1*). P values DT vs Ctrl: *Pepck*, $P = 0.2303$; *Pcx*, $P = 0.095$; *G6pase*, $P = 0.8775$; *Glut1*, $P = 0.0534$. Only male mice were used. All data are shown as mean ± s.e.m.; P values are from two-tailed Mann–Whitney tests.

the glucose-stimulated insulin secretion response in perfused pancreatic slices[22] (Fig. 5a). Pancreatic slices from β-only mice had the same insulin secretion pattern as those containing intact islets from controls (Fig. 5b and Extended Data Fig. 8). In addition, a normal glucose-stimulated insulin secretion profile was also observed in islets isolated from β-only mice (Fig. 5c,d and Extended Data Fig. 8). These results revealed that the biphasic insulin secretion profile is conserved in islets exclusively composed of β-cells. Moreover, the potentiation of glucose-stimulated insulin secretion by exendin-4 (Ex-4, a GLP-1 agonist) was similar in isolated intact and β-only islets (Fig. 5e and Extended Data Fig. 8). Furthermore, β-only and control islets displayed the same mitochondrial respiratory capacity to increase the oxygen consumption rate (OCR) in response to glucose, with similar basal and maximal OCRs (Fig. 5f and Extended Data Fig. 8). Thus, maintenance of the β-cell secretory response correlates with the capacity to effectively engage oxidative phosphorylation for glucose oxidation in the absence of islet α-cells, δ-cells and γ-cells. The regular β-cell function in β-only mice was further supported by the unaltered gene expression and identity of β-cells under fasting or refed conditions (Extended Data Fig. 9).

Next, we wondered whether islets containing only β-cells could enhance their secretory capacity under pathophysiological conditions, such as an extreme insulin demand. For this purpose, the insulin receptor antagonist S961 (ref. 12) was dispensed using an osmotic pump

https://doi.org/10.1038/s42255-024-01114-8

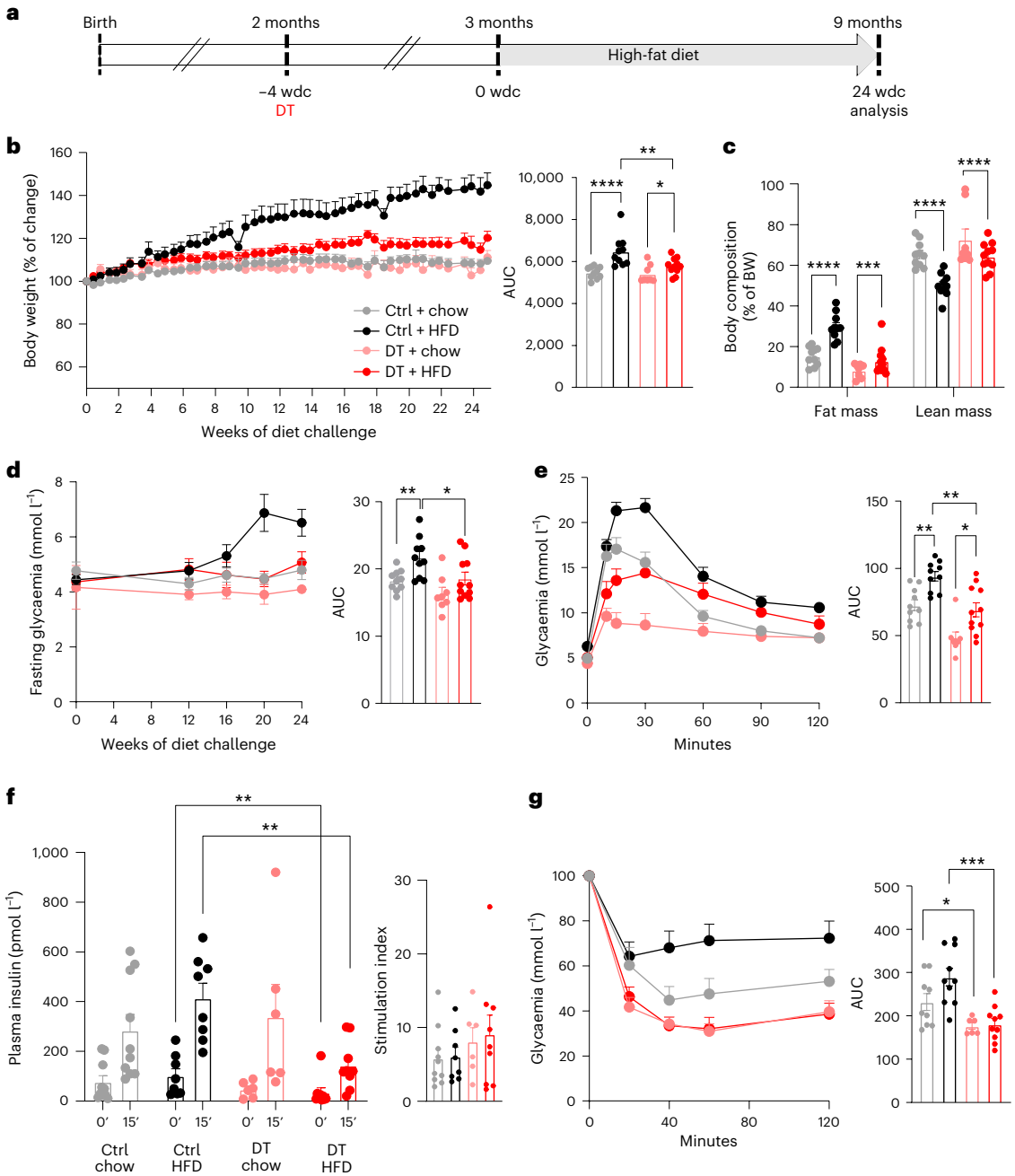

Fig. 4 | Restricted body weight gain and better glucose homeostasis in β-only mice under HFD. a, Experimental design; wdc, weeks of diet challenge. **b**, Percentage of body weight change in Ctrl + chow ($n = 10$), Ctrl + HFD ($n = 10$), DT + chow ($n = 8$) and DT + HFD ($n = 11$). Right panel: AUC of body weight change. *P* values: Ctrl + chow vs Ctrl + HFD, ****$P < 0.0001$; Ctrl + chow vs DT + chow, $P = 0.44$; DT + chow vs DT + HFD, *$P = 0.03$; Ctrl + HFD vs DT + HFD, **$P = 0.007$. **c**, Body composition (fat and lean mass, as % of body weight (BW)) in Ctrl + chow (gray, $n = 10$), Ctrl + HFD (black, $n = 10$), DT + chow (pink, $n = 8$) and DT + HFD (red, $n = 11$). *P* values: fat mass, Ctrl + chow vs Ctrl + HFD, ****$P < 0.0001$; Ctrl + HFD vs DT + HFD, $P = 0.0003$; lean mass, Ctrl + chow vs Ctrl + HFD, ****$P < 0.0001$; Ctrl + HFD vs DT + HFD, $P < 0.0001$. **d**, Fasting glycaemia of Ctrl + chow (gray, $n = 10$), Ctrl + HFD (black, $n = 10$), DT + chow (pink, $n = 8$) and DT + HFD (red, $n = 11$). Right panel: AUC of fasting glycaemia. *P* values: Ctrl + chow vs Ctrl + HFD, **$P = 0.0089$; Ctrl + HFD vs DT + HFD, *$P = 0.0207$. **e**, oGTT at 24 wdc of Ctrl + chow (gray, $n = 10$), Ctrl + HFD (black, $n = 10$), DT + chow (pink, $n = 8$), DT + HFD (red, $n = 11$) mice. Right panel: AUC of oGTT. *P* values: Ctrl + chow vs Ctrl + HFD, **$P = 0.0015$; DT + chow vs DT + HFD, *$P = 0.0068$; Ctrl + HFD vs DT + HFD, **$P = 0.0028$. **f**, Plasma insulin along oGTT. Left panel, plasma insulin 0 and 10 min after glucose injection in Ctrl + chow ($n = 10$), Ctrl + HFD ($n = 8$), DT + chow ($n = 6$), DT + HFD ($n = 9$). Right panel: stimulation index of insulin release. *P* values: Ctrl + chow (0 vs 10 min), $P = 0.0052$; Ctrl + HFD (0 vs 10 min), $P = 0.0006$; DT + chow (0 vs 10 min), $P = 0.0043$; DT + HFD (0 vs 10 min), $P = 0.004$. Ctrl + HFD vs DT + HFD at 0 min, **$P = 0.0056$; Ctrl + HFD vs DT + HFD at 10 min, **$P = 0.0025$. **g**, ITT at 24 wdc. Left panel, ITT as % of change relative to time 0 in Ctrl + chow (gray, $n = 9$), Ctrl + HFD (black, $n = 10$), DT + chow (pink, $n = 6$) and DT + HFD (red, $n = 10$). Right panel: AUC of ITT. *P* values: Ctrl + chow vs DT + chow, *$P = 0.0496$; Ctrl + HFD vs DT + HFD, ***$P = 0.0005$. Body weight changes, body composition, fasting glycaemia, oGTT, plasma insulin levels and ITT were obtained from the same mice. Only male mice were used. All data are shown as mean ± s.e.m.; *P* values are from two-tailed Mann–Whitney tests.

to impose chronic hyperglycaemia (around 30 mM) in control and β-only mice. Both groups behaved similarly and became overtly hyperglycaemic (Fig. 6a) and drastically increased their insulin secretion levels (Fig. 6b). Interestingly, the S961-induced β-cell proliferation was enhanced in β-only islets as compared to controls (Fig. 6c,d). Altogether, these results indicate that β-cell nutrient sensing and secretion

https://doi.org/10.1038/s42255-024-01114-8

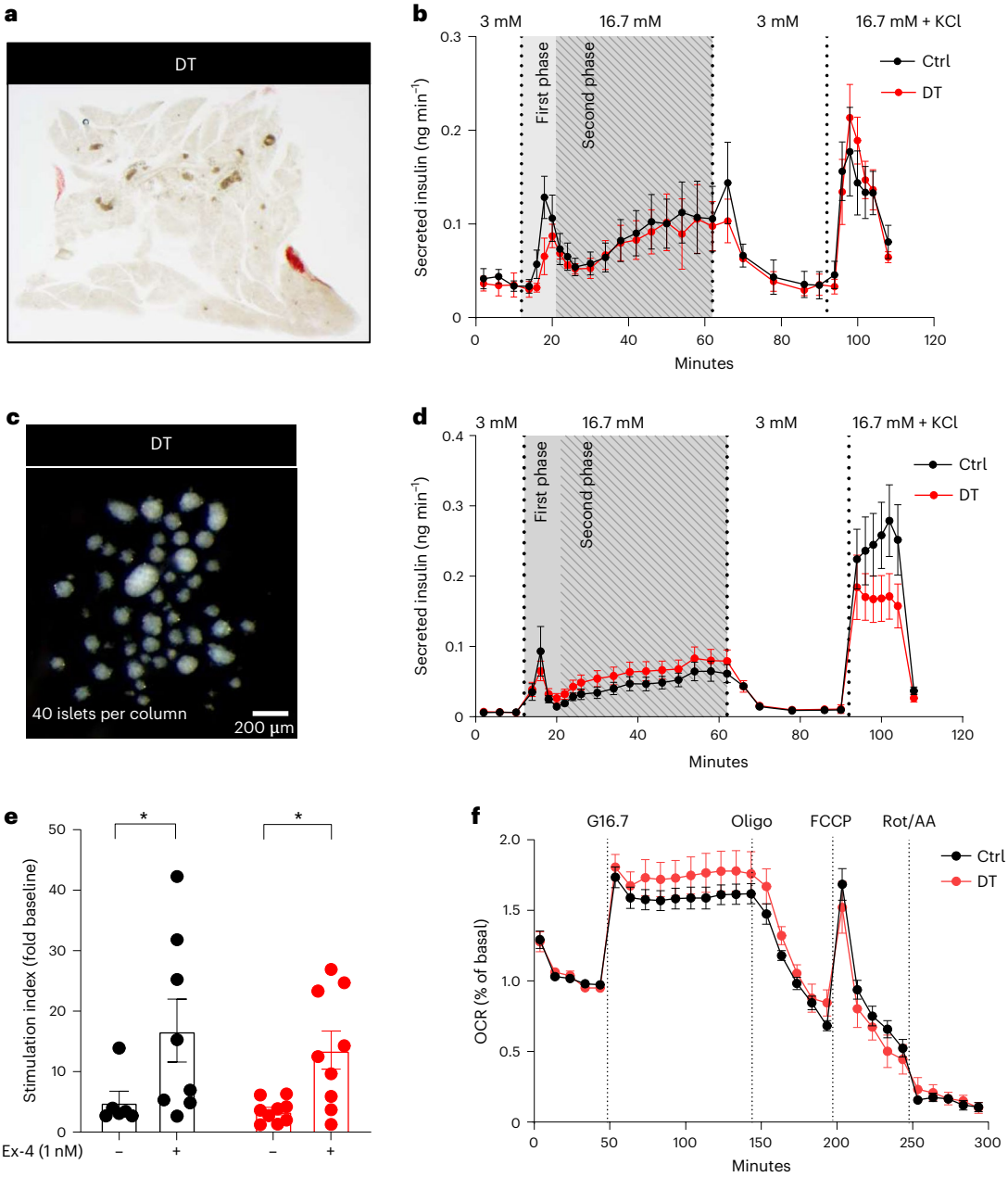

Fig. 5 | Monotypic β-only islets have normal dynamic insulin secretion and islet respirometry. a, Representative picture of a β-only mouse pancreas slice. **b**, Dynamic insulin secretion profiling on pancreatic slices from Ctrl ($n = 5$) and DT ($n = 3$) mice. Gray background area indicates the first and second phase of insulin release. **c**, Representative picture of isolated islets of β-only mice. **d**, Dynamic glucose-stimulated insulin secretion profiling on isolated islets. Absolute insulin secretion from Ctrl ($n = 9$) and DT ($n = 8$) mice. Gray background area represents the first and second phase of insulin release. **e**, Stimulation index (as fold change to baseline values) of in vitro glucose-stimulated insulin secretion in isolated islets of Ctrl (black, $n = 7$) and DT (red, $n = 9$) mice in the presence or absence of the GLP-1 agonist Ex-4. Low glucose is 3 mM; high glucose is 16.7 mM. *P* values: Ctrl with vs without Ex-4, $^*P = 0.048$; DT with vs without Ex-4, $^*P = 0.018$. **f**, Islet respirometry by Seahorse XF96 bioanalyser. Figure shows representative OCR traces of islets from Ctrl ($n = 8$ mice) and DT ($n = 7$ mice) sequentially exposed to 16.7 mM glucose (G16.7), 2.5 µM oligomycin (Oligo), 2 µM FCCP and 3 µM Rot/AA at the indicated time points. Basal measurement was performed at 3 mM glucose before injections. OCR was normalized by insulin content of each well and represented as % of basal. Two to four wells per mouse, eight to ten islets per well. Two-way ANOVA with Sidak's multiple comparisons test. Only male mice were used. All data are shown as mean ± s.e.m. Unless otherwise indicated, *P* values are from two-tailed Mann–Whitney tests.

are appropriately regulated under physiological and extreme insulin needs in mouse islets lacking α-cells, δ-cells and γ-cells.

Human β-cell pseudoislets display optimal insulin secretion

To assess whether human β-cells also maintain their glucose sensing and insulin secretory capacities in the absence of α-cells, δ-cells and γ-cells, we generated human 'islet-like' cell clusters, termed pseudoislets, composed of either all the islet cell types ('control pseudoislets') or only fluorescence-activated cell sorting (FACS)-sorted β-cells (monotypic 'β-pseudoislets'; Fig. 7a and Extended Data Fig. 10). A sharp reduction in *GCG*, *SST* and *PPY* mRNAs, but not *INS* mRNA, was observed in monotypic β-pseudoislets compared with control pseudoislets (Fig. 7b). Accordingly, GCG^+, SST^+ and PPY^+ cells were not detectable in β-pseudoislets (Fig. 7c).

Monotypic β-pseudoislets showed glucose-regulated insulin secretion, with levels similar to control pseudoislets at basal and

https://doi.org/10.1038/s42255-024-01114-8

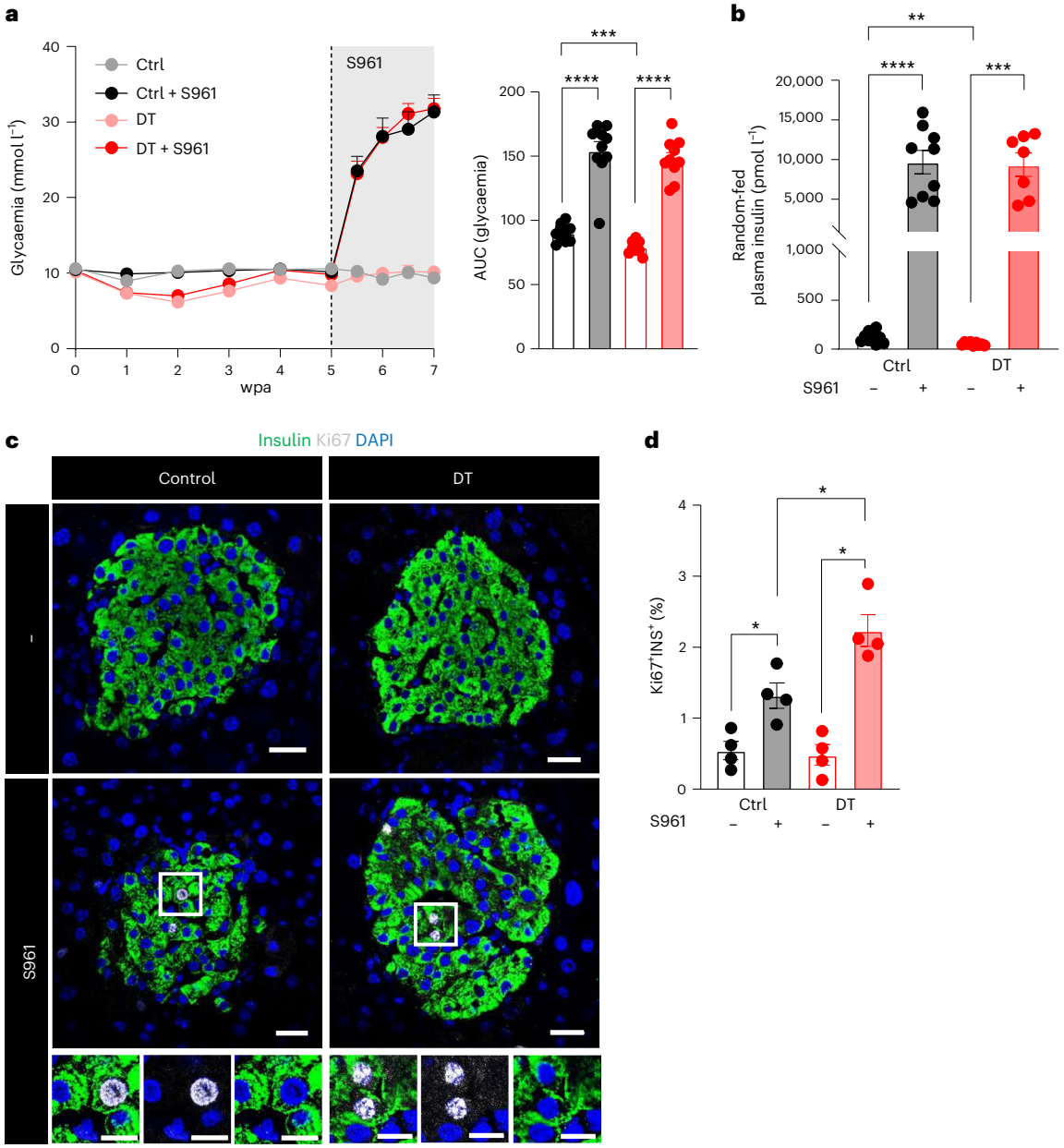

Fig. 6 | Monotypic β-only islets have a normal response to extreme insulin demand. a, Glycaemia before and 2 weeks after S961 treatment on Ctrl ($n = 10$), Ctrl + S961 ($n = 9$), DT ($n = 9$) and DT + S961 ($n = 10$). Right panel: AUC of glycaemia. *P* values: Ctrl vs DT, ***$P = 0.001$; Ctrl vs Ctrl + S961, ****$P < 0.0001$; DT vs DT + S961, ****$P < 0.0001$; Ctrl + S961 vs DT + S961, $P = 0.1903$. **b**, Plasma insulin release under random-fed conditions in Ctrl (gray, $n = 10$), Ctrl + S961 (black, $n = 9$), DT (pink, $n = 9$) and DT + S961 (red, $n = 9$). *P* values: Ctrl vs DT, **$P = 0.0015$; Ctrl vs Ctrl + S961, ****$P < 0.0001$; DT vs DT + S961, ***$P = 0.0002$; Ctrl + S961 vs DT + S961, $P = 0.9182$. **c**, Immunofluorescence on pancreatic sections from Ctrl or DT-treated β-only mice with or without S961 treatment. INS, green; Ki67, gray; DAPI, blue. Scale bars, 20 µm. **d**, Percentage of double-positive INS^+KI67^+ in INS^+ population in Ctrl ($n = 4$), Ctrl + S961 ($n = 4$), DT ($n = 4$) and DT + S961 ($n = 4$). *P* values: Ctrl vs DT, $P = 0.6857$; Ctrl vs Ctrl + S961, *$P = 0.286$; DT vs DT + S961, *$P = 0.286$; Ctrl + S961 vs DT + S961, *$P = 0.286$. Only male mice were used. All data are shown as mean ± s.e.m. *P* values are from two-tailed Mann–Whitney tests.

stimulatory glucose concentrations (Fig. 7d). When further challenged with Ex-4, β-pseudoislets secreted more insulin than control pseudoislets (Fig. 7d), indicating a potentiation of the incretin response in the absence of α-cells, δ-cells and γ-cells. Similar results were obtained when assessing the stimulatory index (Extended Data Fig. 10). Like mouse β-only islets, human β-pseudoislets showed no significant differences in islet respirometry parameters compared to control pseudoislets (Fig. 7e and Extended Data Fig. 10). Thus, glucose-stimulated insulin secretion from human β-pseudoislets is closely correlated with their capacity to increase mitochondrial respiration in response to glucose (Fig. 7d,e and Extended Data Fig. 10). Altogether, these results indicate that human β-cells, like mouse β-cells, can sense glucose and secrete insulin in a regulated manner in the absence of α-cells, δ-cells and γ-cells.

Discussion

We describe a mouse model in which the adult pancreatic islets are exclusively made up of β-cells. The near total loss of non-β-cells in these mice does not affect their viability, motor and feeding behaviour, body weight or blood glucose homeostasis (fasting and random fed). This correlates with—and could be explained, at least in part by—the persistence of circulating SST and GCG after non-β-cell

https://doi.org/10.1038/s42255-024-01114-8

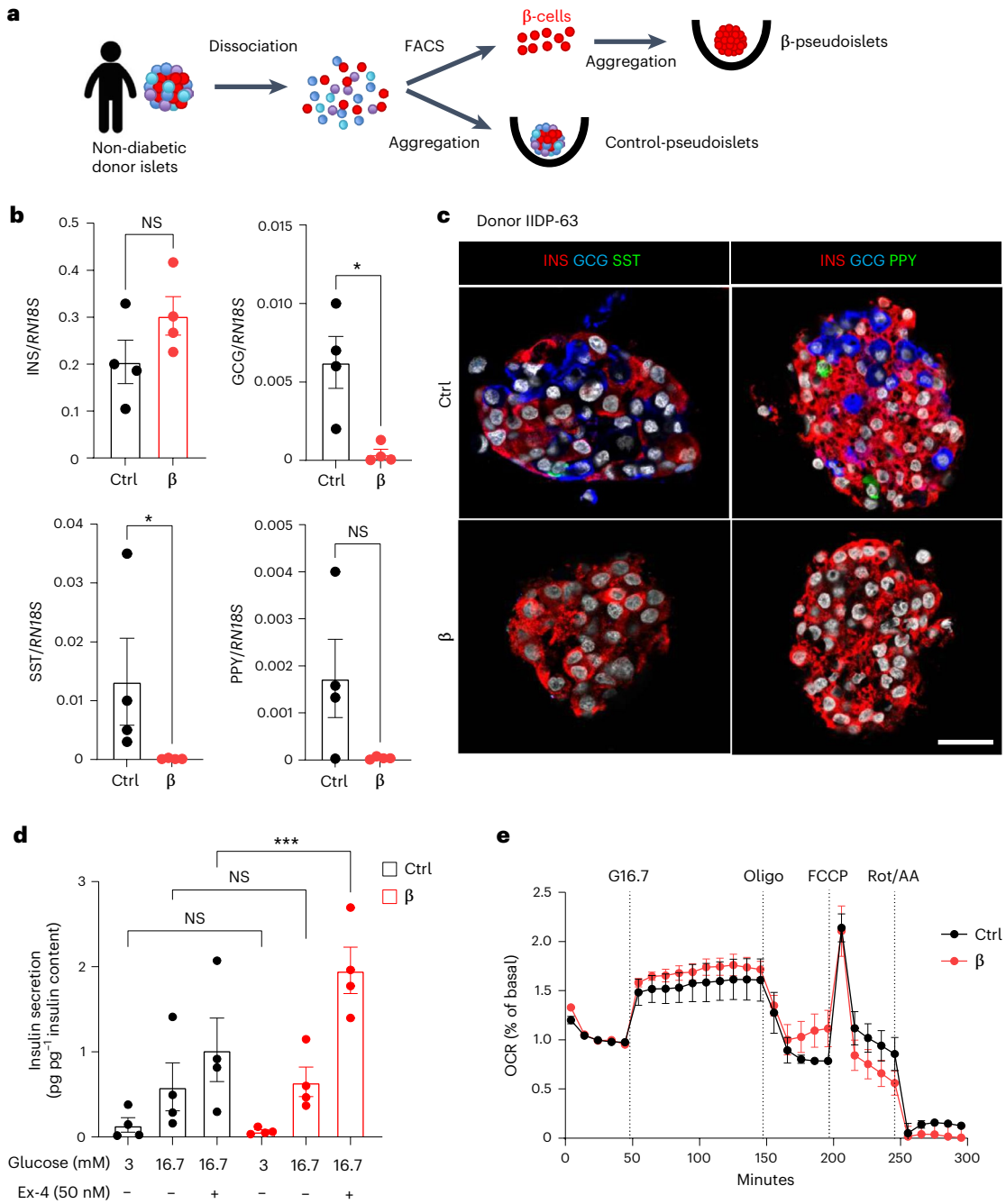

Fig. 7 | Human monotypic β-pseudoislets maintain glucose-stimulated insulin secretion and islet respirometry. a, Generation of human pseudoislets. Islets from the same donor were dissociated and sorted by FACS to obtain highly pure β-cells that were aggregated into pseudoislets. Control pseudoislets comprising all cell types were dissociated and aggregated directly. **b**, qPCR of *INS*, *GCG*, *SST* and *PPY* on control and β-pseudoislets. Data are normalized to housekeeping genes (*RN18S*); $n = 4$ donors. *P* values (Ctrl vs β): *INS*, $P = 0.200$; *GCG*, $^*P = 0.0286$; *SST*, $^*P = 0.0286$; *PPY*, $P = 0.1714$. NS, not significant. **c**, Immunofluorescence on control pseudoislets (Ctrl) or monotypic β-pseudoislets (β). INS, red; GCG, blue; SST, green (left); INS, red; GCG, blue; PPY, green (right). Scale bar, 20 µm. **d**, In vitro insulin secretion normalized by total insulin content in Ctrl and monotypic β-pseudoislets assessed at basal (3 mM, low glucose (LG)) or stimulatory (16.7 mM, high glucose (HG)) glucose concentrations in the presence or absence of the GLP-1 agonist Ex-4. $n = 4$ donors. *P* values (Ctrl vs β): LG, $P = 0.1831$; HG, $P > 0.999$; HG + Ex-4, $^{***}P = 0.0002$. NS, not significant. **e**, Islet respirometry by Seahorse XF96 bioanalyser. OCR traces of human Ctrl or β-only pseudoislets. Glucose (16.7 mM; G16.7), oligomycin (2.5 µM; Oligo), FCCP (2 µM) and Rot/AA (3 µM) were injected at the indicated time points. Basal measurement was performed at 3 mM glucose before injections. OCR was normalized by insulin content of each well and represented as % of basal. $n = 3$ independent donors. Two to five wells per condition per donor, ten pseudoislets per well; Two-way ANOVA with Sidak's multiple comparisons test. Both male and female human donors were used. All data are shown as mean ± s.e.m. Unless otherwise indicated, *P* values are from two-tailed Mann–Whitney tests.

ablation. The modest decrease in glucagonaemia, which was previously described in mice lacking α-cells only[15,20], along with the preserved counter-regulatory actions of cortisol, epinephrine and/or growth hormone, probably prevent mild hypoglycaemia, as reported in mice with constitutive and complete GCG signalling abrogation[3,21]. We could not assess blood PPY levels owing to the absence of reliable commercial kits, yet the fact that PPY knockout mice remain normoglycaemic in both homeostatic[14] and HFD[23] conditions suggests that

PPY is dispensable for blood glucose homeostasis. We also evaluated ex vivo the intrinsic capacity of islets devoid of α-cells, δ-cells and γ-cells to secrete insulin in response to glucose independently of the influence of peripheral tissues. Surprisingly, we found that pancreatic slices and isolated islets composed exclusively of β-cells exhibit insulin secretion dynamics similar to that of intact islets, with preserved first and second secretion phases upon glucose stimulation. This correlates with the transcriptomic and mitochondrial respiration analyses, which did not show major changes in β-cell identity and glucose metabolism.

Our results reveal an unexpected consistent improvement of insulin sensitivity and glucose tolerance in β-only mice of both genders. Coincidentally, although plasmatic GCG levels were moderately reduced after non-β-cell ablation, improved glucose tolerance associated with increased GLP-1 levels, better insulin sensitivity and restricted HFD-induced weight gain were also previously reported under extreme conditions of GCG signalling blockade[3] (GCGR KO and GCGR-neutralizing antibody treatment).

Single-islet cell-type ablation (either α-cells, δ-cells or γ-cells; Supplementary Table 1) did not fully recapitulate the metabolic phenotype of β-only mice. The α-cell or γ-cell ablated mice did not exhibit an obvious metabolic phenotype, as previously shown[14,15]. However, the absence of δ-cells led to a mild reduction of blood glucose levels (Extended Data Fig. 4), as it was previously shown in a similar mouse model of δ-cell ablation[24] and in *Sst*[25] or *Hhex*[26] null mice. The defects in β-cell function and blood glucose homeostasis associated with the absence of δ-cells are somehow compensated by the simultaneous removal of α-cells and γ-cells in β-only mice. We thus reason that the combined loss of all non-β cells may imbalance systemic hormone signalling (that is, the insulin/GCG ratio and GLP-1 levels, among others), triggering compensatory or adaptive mechanisms in peripheral organs such as the liver and WAT, which may explain the observed improved insulin sensitivity and fatty acid metabolism. The increased GLP-1 levels triggered by non-β-cell loss may participate in the phenotype of β-only mice under homeostatic and HFD conditions, as this intestinal incretin is an important regulator of blood glucose homeostasis through potentiation of glucose-stimulated insulin secretion[27–29], suppression of hepatic gluconeogenesis or glycogenolysis and of GCG secretion, satiety stimulation and improvement of insulin sensitivity[27–31]. In addition, GLP-1 receptor agonists enhance insulin sensitivity in hepatic and adipose tissues and reduce obesity in diabetic animals and humans[32–36]. Of note, the improved insulin sensitivity in β-only mice might be a result of the slightly lower basal insulin secretion observed in vivo after removal of the three islet cell types. This subtle decrease in basal insulin secretion may trigger better insulin sensitivity as an adaptive phenomenon. However, defining the precise contribution of each peripheral organ in the phenotype of β-only mice is difficult owing to the dynamic and complex interplay between the different tissues involved in glucose homeostasis and lipid metabolism. Overall, intra-islet interactions are superimposed to inputs from peripheral tissues and integrated within the islet network to minutely regulate the β-cell secretory activity.

The ability of β-cells to increase their secretion capacity in response to incretin potentiators or extreme insulin demand, such as GLP-1 receptor agonist or an insulin receptor blockade, was maintained in β-only mice. These observations were repeated with human β-cells, whereby the glucose-stimulated insulin secretion and the mitochondrial respiration capacity were preserved in β-pseudoislets. Interestingly, it has been postulated that GLP-1 secreted by human α-cells is required for regulated and synchronous insulin secretion from β-cells[37,38], yet here we show that human β-only pseudoislets maintain the incretin-stimulated insulin secretion like pseudoislets composed of all islet cell types.

Although α-cells, δ-cells and γ-cells unequivocally participate in the regulation of β-cell function, it is astonishing that both murine and human islets maintain proper insulin secretion in their absence. This optimal glucose-regulated insulin secretion strongly suggests that connectivity and communication of β-cells among themselves is crucial whereas the heterologous interactions between β-cells and non-β-cells are not. β-cells are functionally coupled through gap junctions among themselves and with non-β-cells within islets[39–41]. Electrical coupling between β-cells is critical to ensure proper insulin secretion[42,43]. Insulin release defects upon disruption of the gap junction connexin 36 illustrate the importance of the electrical coupling between β-cells for their synchronization, controlled intracellular Ca^{2+} oscillations and proper insulin secretory activity[42–44]. The genetic or pharmacological inhibition of connexin 36 causes the loss of oscillatory insulin secretion[44,45]. Reaggregation of purified isolated primary human β-cells in cell clusters devoid of α-cells, δ-cells and γ-cells restores glucose-stimulated insulin secretion as compared to dispersed cells[13,46], supporting the notion that β-cell connectivity is key for regulated secretion activity in different species. In this context, human islet α-cells, δ-cells and γ-cells are intermingled among β-cells (which represent 50% of the islet cell mass), implying that most of the β-cells physically interact with non-β-cells[47–49]. Conversely, in mouse islets, non-β-cells are mainly located at the islet periphery surrounding a central core of β-cells (representing 75% of the islet mass), an architecture that favours homotypic associations between β-cells over β-cell–non-β-cell interactions[48,50]. The variable proportions and spatial distribution of the different islet cell types across species, together with the non-β-cell ablation data reported here, suggest that β-cell–non-β-cell direct interactions are not crucial to ensure properly regulated insulin secretion, contrary to what was thought so far.

Our results reveal that non-β-cells, when concomitantly lost, do not appear to be essential to ensure β-cell function in homeostatic or stress conditions, such as extreme insulin demand. Therefore, one wonders why adult pancreatic islets have α-cells, δ-cells and γ-cells. One possibility is that these cells had essential functions during evolution, but became somewhat 'redundant' as evolution progressed. For instance, GCG-expressing α-cells may have evolved as part of an essential counter-regulatory mechanism to cope with long periods of starvation and energy deficit. However, the presence of alternative counter-regulatory hormones could have attenuated the requirement of α-cells through evolution. Still, the lack of δ-cells impacts the threshold for glucose-stimulated insulin release[24], suggesting that the absence of this single cell type cannot be compensated, unless all non-β-cells are simultaneously depleted. Alternatively, or in addition, α-cells, δ-cells and γ-cells may have a direct role as supporting cells during embryonic development and perinatal maturation of β-cells[51,52]. In line with this notion, a previous study showed that ablation of embryonic SST-expressing cells results in increased insulin content and excessive insulin release leading to severe hypoglycaemia and neonatal death[53]. Yet other reports do not support a developmental role for embryonic δ-cells on β-cell maturation[52,54]. Depletion of *Ppy*-expressing cells in mouse embryos led to a significant reduction in pancreatic insulin-containing and SST-containing cells, suggesting that the presence of γ-cells is crucial for β-cell and δ-cell differentiation[55,56]. Likewise, GCG signalling was also shown to be critical for proper islet development and maturation[57].

Although defects in β-cell function and identity are clearly associated with diabetes, mounting evidence supports that the activity of non-β-cells is compromised in this condition. Although it is not clear how non-β-cells precisely contribute to disease progression and insulin secretion defects, our findings support that the absence of dysfunctional non-β-cells or strategies aimed at abrogating aberrant signalling from these cells would confer beneficial therapeutic effects in diabetes[11,58–60]. It has been shown that α-cell dysfunction occurs at early stages of islet autoimmunity, before diabetes onset[61–63]. Ongoing clinical trials are exploring the effect of GCGR antagonists on the hyperglucagonaemia typical of diabetic patients[64–67]. Interestingly, insufficient secretion of GCG in response to hypoglycaemia in

type 1 diabetes increases the risk of hypoglycaemic episodes under insulin therapy[68,69]. In diabetic rodents, restoration of GCG levels during hypoglycaemia was described upon administration of SST receptor antagonists[70,71], suggesting that perturbed SST secretion could have a role in the absence of counter-regulatory response in diabetes[72,73].

At present, multiple therapeutic strategies are aimed at generating, either in vitro or in situ, insulin-producing β-like cells[74,75]. The preserved glucose-stimulated insulin secretion in pancreatic islets made exclusively of β-cells, which is also found in aged mice and human cells, suggests that non-β-cells are dispensable for β-cell function. This supports current efforts aimed at generating functional surrogate β-like cells from stem cells[76], with particular attention to establishing adequate β-cell identity and cellular connectivity. These observations also clarify concerns about the decreased non-β-cell mass in situations whereby massive non-β-cell recruitment into insulin production and secretion was achieved to treat diabetes[74,77,78].

Methods

Animals

To generate the Sst-DTR knock-in mice, we used a CRISPR ribonucleoprotein complex containing the Cas9 protein along with the following two gRNAs: 5′-CAGGGCGCACTGGAGACGGC-3′ and 5′-ACAACAATATTAAAGCTAAC-3′ to target the SST locus. The donor plasmid (pBluescript II SK+) contained the DTR sequence flanked by a 2 kb right homology arm (upstream of the ATG in the Sst locus) and a 2 kb left homology arm (downstream of the STOP codon in the Sst locus). The ribonucleoprotein complex was co-injected with the donor plasmid in one-cell embryos. To generate this transgenic mouse model, the Sst-DTR transgene was combined with the previously described Gcg-DTR and Ppy-DTR transgenes. The non-β-DTR mice had a mixed genetic background.

Mice were housed in open cages, with densities varying depending on the size of the cage, in accordance with the Swiss regulation (Cage type S to L, Charles River). Cages were enriched with bedding, nestlet and a mouse house. Temperature and humidity in the housing room were maintained at 20–24 °C and 30–70%, respectively. The day–night cycles were programmed by alternating 12 h day and 12 h night. Animals received food and tap water ad libitum. Both male and female mice were used for experiments. Animals were randomly allocated to control or treatment groups. The study followed all ethical regulations regarding animal experimentation, and all experiments were performed under the guidelines of the Direction General de la Santé du Canton de Genève (license numbers GE/111/17, GE/121/17 and GE15820).

DT and S961 treatment

DT (Sigma-Aldrich) was injected intraperitoneally (126 ng of DT per injection on days 0, 1 and 2, or 5 ng of DT per injection on days 0, 3 and 6) to 2-month-old mice. S961 (Novo Nordisk) was given by ALZET osmotic pumps implanted subcutaneously (40 nmol per week).

Human islets and generation of human pseudoislets

All studies involving samples of human tissues were approved by the ethical committee of the University of Geneva. Human pancreatic islets were obtained from the Geneva University Hospital (Geneva, Switzerland), from the National Institute of Diabetes and Digestive and Kidney Diseases (NIDDK)-funded Integrated Islet Distribution Program (IIDP) at Beckman Research Institute of City of Hope (Duarte, CA, USA) and from the University of Alberta Diabetes Institute IsletCore (Edmonton, Alberta, Canada). All donors' families gave informed consent for the use of pancreatic tissue in research. Subjects were de-identified at the source of organ procurement, whereby samples were assigned a unique identifier or RRID to ensure privacy. Donors' unique identifiers and basic metabolic details are described in Supplementary Table 4.

Upon arrival, islets were cultured overnight in fresh CMRL 1066 media (11530-037, Gibco) at 37 °C and 5% CO_2. Dissociation of human islets and staining with cell-surface antibodies to purify β-cells was performed as described previously[13,79]. Stained cells were sorted on a Moflo Astrios (Beckman Coulter) system. Single viable islet cells were gated by forward-scatter, side-scatter and pulse-width parameters and by negative staining for DAPI (Invitrogen, D1306) to remove doublets and dead cells. For the formation of pseudoislets, agarose structures with spherical microwells were obtained by using a micro-mold (3D Petri Dish, Microtissues) and then used to promote self-assembly of the cells in a density of 1,000 cells per pseudoislet. Every other day, the culture media was changed. Experiments were performed 7 days after culture. Pseudoislet morphology and cell composition were evaluated by immunostaining and quantitative PCR with reverse transcription (RT–qPCR), as detailed below.

Islet isolation, FACS and RNA extraction

Islets were isolated from previously reported *Insulin-mCherry* mice, whose insulin-producing cells constitutively express mCherry[12]. Cell sorting using FACS was performed as described in previous works[10,12,14] using a Moflo Astrios (Beckman Coutler) system with Summit v.6.2 (Beckman Coulter) software. Kaluza Analysis v.2.0 (Beckman Coulter) software was used for subsequent analyses. Islets were frozen in RLT buffer (Qiagen) with β-mercaptoethanol and stored at −80 °C before being processed for RNA extraction. RNA extraction from islets was performed using the Qiagen RNeasy Micro Kit. RNA extraction from tissue (duodenum, brain or liver) was performed using the Qiagen RNeasy Plus Universal Mini Kit.

RT–qPCR

Complementary DNA (cDNA) of total mouse islets, human pseudoislets, duodenum, liver and/or brain fractions was generated using the Qiagen QuantiTect Reverse Transcription Kit. qPCR reactions were performed using the appropriate primer mixes for each gene as well as the Express SyBr GreenER kit (Invitrogen, 100001652). We used the CorbettRobotics4 robot, and the PCR reaction was completed in the CorbettResearch6000 series cycler using a 40 cycles program. Normalization and analysis of the data were done with the RT–PCR analysis_macro v.1.1 (the Genomic Platform, University of Geneva) using two normalization genes (*Gapdh* and *β-actin*). Samples were run in triplicate. For human pseudoislets, biological duplicates of each sample were run in triplicate. Expression levels were normalized to *RN18S*. Primer sequences are shown in Supplementary Table 2.

Bulk RNA sequencing

β-cells were FACS-sorted from 1-month post-ablation and control mice, either under fasting or fasting plus 2 h refed condition. Islets were isolated and dissociated as described above. RNA was extracted as described above and assessed for quality by an Agilent bioanalyser before library generation and sequencing. Library preparation, RNA sequencing and quality controls were performed in the Genomics Core Facility of the University of Geneva. Reverse transcription and cDNA amplification were performed using the SMARTer Ultra Low RNA Kit (Clontech). cDNA libraries were prepared using Nextera XT DNA Sample Preparation Kit (Illumina) and sequenced on an Illumina HiSeq4000 platform with single-end 100-bp reads.

Analyses were performed following previously established pipelines[14]. All sequencing data were uploaded to and aligned on the Galaxy project[80] against Ensembl reference genome GRCm38.p6 (release 100) using STAR version 2.7.2b[81] in two-pass mapping mode. Aligned data were counted using HTSeq v.0.9.1 (ref. 82) in union mode. Analyses were performed in a pairwise manner between the four conditions analysed using DESeq2 v.1.28.1 (ref. 83). For each pairwise comparison, genes were discarded if they had fewer than five counts per sample on average. After calculating differential expression between groups,

log_2(fold changes) were shrunken using the normal estimator[83]. Genes were considered to be differentially expressed if the absolute shrunken log_2(fold changes) were ≥1 and adjusted *P* values were ≤0.05.

A previously generated β-ID gene list[79] was used to identify possible changes in identity and gene expression in β-cells after non-β-cell ablation.

Glucose tolerance test

Mice were fasted for 16 h before starting the experiments. Intraperitoneal or oral glucose tolerance tests were performed as previously described[9]. A 20% glucose solution was injected intraperitoneally or through gavage to fasted mice relative to their body weight. Glycaemia was measured before the injection and 15, 30, 60, 90 and 120 min after glucose administration.

Insulin tolerance test

Mice were intraperitoneally injected with insulin (0.5 U kg^{-1} or 0.4 U kg^{-1} for the HFD experiment; Actrapid, Novo Nordisk) after 5 h of fasting. Glycaemia was measured before and 20, 40 and 60 min after injection.

Tissue protein extracts

Pancreatic or intestinal tissues were homogenized in acid–ethanol solution (74% ethanol, 1.4% HCl), then sonicated and centrifuged. The supernatant was collected and used for the immunoassay experiments, which were performed following the manufacturer's instructions (Mercodia Ultrasensitive Mouse Insulin ELISA 10-1249-01; Mercodia Glucagon ELISA 10-1281-01).

Brain tissue was homogenized in a lysis buffer containing 10× Cell Lysis Buffer (Cell Signaling, 9803), PMSF (Cell Signaling, 8553) and distilled water (dH_2O; BioConcept, 3-07F04-I), then sonicated and centrifuged. The supernatant was collected and used for immunoassay experiments, which were performed following the manufacturer's instructions (Phoenix Peptide Somatostatin Fluorescent EIA Kit, EK-060-03).

Plasma hormone measurements

Insulin (Mercodia Ultrasensitive Mouse Insulin ELISA, 10-1249-01), GCG (Mercodia Glucagon ELISA, 10-1281-01), GLP-1 (Millipore Multi Species GLP-1 Total ELISA, EZGLP1T-36K), cortisol (R&D Systems Cortisol Parameter Assay Kit, KGE008B), growth hormone (Alpco Mouse/Rat Growth Hormone ELISA, 22-GHOMS-E01) and epinephrine (LSBio Mouse Adrenaline/Epinephrine ELISA Kit, LS-F28134) were measured in plasma samples obtained from blood extracts from the tail vein or cardiac puncture. A dipeptidyl peptidase 4 inhibitor (Merck, DPP4) was added to the blood samples to avoid GLP-1 degradation. All analyses were performed following the manufacturer's instructions.

Hepatic glycogen assay

Approximately 30 mg of liver tissue was homogenized and boiled for 5 min. After centrifugation at 13,000*g* for 5 min at 4 °C, at least 50 µl of supernatant was collected for analysis. Glycogen was assessed using the Glycogen Assay Kit (Merck, MAK016-1KT).

Hepatic pyruvate and lactate assay

Approximately 30 mg of liver tissue was lysed in a solution of 10× Cell Lysis Buffer (Cell Signaling, 9803), PMSF (Cell Signaling, 8553) and dH_2O (BioConcept, 3-07F04-I), deproteinized in PCA (BioVision, K808-200) and neutralized (BioVision, K808-200) following the manufacturer's instructions. Pyruvate (BioVision, K609-100) and lactate (BioVision, K607-100) were analysed following the manufacturer's instructions.

Immunofluorescence

Paraffin and cryosections were 5 and 10 µm thick, respectively. The primary antibodies used were guinea pig anti-insulin (1:400; DAKO, A0564), rabbit anti-insulin (1:3,000; Molecular Probes, 701265), chicken anti-insulin (1:200; Abcam, ab14042); mouse anti-glucagon (1:1,000; Sigma-Aldrich, G2654), rabbit anti-glucagon (1:200; DAKO, A0565), mouse anti-somatostatin (1:200; BCBC, Ab1985), rabbit anti-somatostatin (1:200; DAKO, A0566), rat anti-somatostatin (1:200; Merck, Mab354) mouse anti-Ppy (1:400; Santa Cruz, MAB62971) and goat anti-Glp1 (1:100; Santa Cruz, sc-7782). Sections were also stained with DAPI. Secondary antibodies were coupled to Alexa 488, 405, 568, 647 (1:500; Molecular Probes) or TRITC (1:500; Southern Biotech). All antibodies are listed in Supplementary Table 3. All sections were examined with a confocal microscope (Leica TCS SPE).

Body composition

Body composition was determined in awake mice by magnetic resonance using EchoMRI-700 (EchoMRI). Body composition is expressed as a percentage of body weight (that is, percent of lean and fat mass).

Hyperinsulinemic–euglycaemic clamp

Hyperinsulinemic–euglycaemic clamps were performed in conscious, unrestrained, catheterized mice as previously described[84]. In brief, catheters were surgically implanted 7 days before the experiment in the right jugular vein and exteriorized above the neck using a vascular access button (Instech Laboratories). Mice were fasted for 3 h, followed by a 2 h infusion of [3-^{3}H] glucose (0.05 µCi min^{-1}) (Perkin Elmer). The basal rate of glucose disappearance (mg glucose kg^{-1} of body weight × min^{-1}) was determined by blood sampling in duplicate. Continuous insulin infusion (2.5 mIU kg^{-1} body weight × min^{-1}; Actrapid, Novo Nordisk) was used after that for the induction of hyperinsulinaemia. At steady state, hepatic glucose production (mg glucose kg^{-1} of body weight × min^{-1}) and the insulin-stimulated rate of glucose disappearance (mg of glucose kg^{-1} of body weight × min^{-1}) were determined by two blood samplings. The in vivo insulin-stimulated glucose uptake in tissues was then determined by a 10 µCi bolus intravenous injection of 2-[^{14}C] deoxyglucose. After 30 min, mice were rapidly killed by cervical dislocation, and tissues were removed and stored at −80 °C until use. Measurements of 2-[^{14}C] deoxyglucose-6-phosphate concentration in individual tissues allowed calculation of the glucose utilization index in tissues. Glycaemia was measured using an Xpress glucometer, and basal and steady-state insulinaemia were determined using a commercial ELISA kit (CrystalChem).

Glucose uptake

In vivo insulin-stimulated glucose uptake in tissues was determined by a 20 µCi bolus intravenous injection of 2-deoxy-[1,2-3H]-glucose (ARC) in the presence of insulin (NovoRapid) at 0.5 IU kg^{-1} intraperitoneally. Blood was sampled from the tail vein 2, 20, 40 and 60 min after injections. After 1 h, mice were killed and tissues were collected and stored at −80 °C until use. Glucose concentration in deproteinized blood samples was measured using the glucose oxidase method (Roche Diagnostics). Measurements of [1,2-3H] deoxyglucose-6-phosphate levels in deproteinized blood samples and individual tissues allowed calculation of the glucose utilization index in tissues.

Islet isolation for perifusion assays

Islets were isolated from the pancreas of 7 h-fasted donor mice by collagenase digestion (0.45 mg ml^{-1}) and purified by a discontinuous Ficoll density gradient. After isolation, islets were hand-picked in RPMI-1640 medium supplemented with 5% (v/v) FCS (Gibco), 1% (v/v) L-glutamine (Gibco), 1% (v/v) penicillin–streptomycin (Sigma-Aldrich) and 5.5 mM glucose (Merck). Islets were allowed to rest free-floating for 18–24 h before islet perifusion assays at 37 °C and 5% CO_2.

Pancreas tissue slices

Pancreas tissue slices were performed on 7 h-fasted mice as described previously[22,85]. In brief, pancreata were injected with 1.25% low-melting-point agarose (Roth) after killing the mouse. After

solidification, the pancreas was excised and embedded in agarose (1.25%). Tissue blocks were subjected to a semiautomated vibratome (Leica) and pancreas tissue slices were cut in ECS solution (125 mM NaCl, 2.5 mM KCl, 26 mM $NaHCO_3$, 1.25 mM NaH_2PO_4, 1 mM $MgCl_2$, 2 mM $CaCl_2$, 10 mM HEPES, 3 mM glucose pH 7.4) at a thickness of 150 µm. Slices were collected into a 6 cm Petri dish containing 3 mM glucose KRBH buffer (137 mM NaCl, 5.36 mM KCl, 0.34 mM Na_2HPO_4, 0.81 mM $MgSO_4$, 4.17 mM $NaHCO_3$, 1.26 mM $CaCl_2$, 0.44 mM KH_2PO_4, 10 mM HEPES, 0.1% BSA, 3 mM glucose pH 7.3) with aprotinin (25 KIU ml^{-1}, Sigma-Aldrich, A6106) and allowed to rest for 120 min at room temperature (20–22°C) while shaking before performing slice perifusion experiments.

Perifusion assays and insulin secretion quantification

Dynamic insulin secretion of isolated islets and pancreas tissue slices was performed using a perifusion system with automated tray handling (Biorep Technologies, PERI4-02-230-FA). A total of 40 islets were placed into perifusion columns (Biorep Technologies, PERI-CHAMBER) according to the provided manual, whereby islets are placed between two layers of sedimented agarose beads. For pancreas tissue slice perifusion, three slices originating from different embedded blocks were placed into a closed perifusion chamber (Warner Instruments, 64-0223 and 64-0281 (P-5)) connected to the perifusion system. To equilibrate the islets or slices to 37 °C and to wash out accumulated hormones and enzymes, a 90-min flushing step with 3 mM glucose KRBH with aprotinin (25 KIU ml^{-1}, Sigma-Aldrich, A6106) at a flow rate of 100 µl min^{-1} was performed. Subsequently, the perifusion protocols were applied using a flow rate of 100 µl min^{-1} and sample collection in 96-well plates at 2-min intervals. Aprotinin (25 KIU ml^{-1}) was added to all KRBH buffers used for the different protocols. After perifusion, islets and slices were recovered from the columns and perifusion chambers and lysed for total insulin content measurement using 250 µl and 500 µl acid–ethanol (2% HCl (37 %, 12 M) in absolute ethanol), respectively. All samples were kept at −20 °C until measured with an Insulin Ultrasensitive HTRF Assay Kit (Perkin Elmer–Cisbio, 62IN2PEH).

In vitro static glucose-stimulated insulin secretion

Murine isolated islets or human pseudoislets were hand-picked for each assay replicate and washed by incubation for 1 h at 37 °C in secretion medium containing 2.5 mM $CaCl_2$, 140 mM NaCl, 4.5 mM KCl, 1 mM $MgCl_2$, 20 mM Hepes and 3 mM glucose (Sigma-Aldrich) in dH_2O. Samples were then transferred into fresh secretion medium containing 3 mM (low) glucose for 1 h, followed by incubation for another 1 h in secretion medium containing 16.7 mM (high) glucose at 37 °C. Then, 1 nM Ex-4 (Sigma-Aldrich, E7144) supplementation in the secretion medium containing 16.7 mM (high) glucose was added to assess the response of β-cells to the incretin agonist. The medium was collected after a 1 h incubation at each glucose concentration and stored at −80 °C for subsequent analysis. Islets and pseudoislets were recovered and lysed for total insulin content using acid–ethanol (74% ethanol, 1.4% HCl). Mouse insulin concentration was quantified using the Ultrasensitive Mouse Insulin ELISA (10-1249-01, Mercodia). Human insulin concentration was measured using the Insulin Chemiluminiscence ELISA (ALPCO, 80-INSHU-CH01).

XFe96 Seahorse islet respirometry

Mouse islets or human pseudoislets (8–10 per well) were seeded into wells of a poly-D-lysine-coated (100 mg ml^{-1}) XFe96 plate containing Seahorse XF base media RPMI (supplemented with 3 mM glucose, 10 mM HEPES, 2 mM glutamax, 30 mM NaCl and 0.1% FBS) as described previously[86]. Before the assay, islets were incubated for 1 h at 37 °C in a non-CO_2 incubator. The Seahorse XFe96 extracellular flux analyser and the Mito Stress kit containing mitochondrial toxins (Agilent Technologies) were used to assess mitochondrial respiration and islet bioenergetics. Basal respiration was first measured at 3 mM glucose. Then, islets and pseudoislets were sequentially stimulated with glucose (final well concentration of 16.7 mM), oligomycin (2.5 µM), FCCP (2 µM) and a mixture of rotenone and antimycin A (Rot/AA, 3 µM). Islets and pseudoislets were recovered at the end of the assay and lysed for total insulin content using acid–ethanol (74% ethanol, 1.4% HCl).

OCR values were normalized by insulin content per well to reduce the confounding effect of non-β-cells in the measurements of the control samples. Then, a fold change to the basal respiration was calculated. Bioenergetics parameters were calculated as previously described[86]. In brief, average values after injection of Rot/AA were subtracted from all OCR measurements. Glucose-stimulated OCR was calculated by dividing the maximum OCR measurement after 16.7 mM glucose injection by the last basal OCR measurement at 3 mM glucose. Proton leak was determined by dividing the minimum OCR value after oligomycin A stimulation by the last basal OCR value. Lastly, maximal respiration was calculated by dividing the maximal OCR value after FCCP injection by the last basal OCR value. All parameters were multiplied by 100 and are shown as % of basal.

HFD

Rodent diet with 60 kcal% fat (Research Diets, D12492) or diet with 10 kcal% fat (Research Diets, D12450J) were administered to control and β-only mice 1 month post ablation, for 24 weeks. The diet was changed every 2 days.

Metabolic cage (Labmaster)

Body mass composition was analysed before and after indirect calorimetric experiment using an EchoMRI-700 (EchoMRI). Mice were analysed for whole energy expenditure, oxygen consumption and carbon dioxide production, respiratory exchange rate (VCO_2/VO_2), food intake and spontaneous locomotor activity using calorimetric cages (Labmaster, TSE Systems). Activity was recorded using an infrared light beam-based locomotion monitoring system (beam breaks per 15 min). Spontaneous exercise activity was also recorded using running wheels (Columbus) inside the metabolic cage. Mice were individually housed and acclimated for 4 days before experimental measurements. Data analysis was carried out with Excel using extracted raw values of the last 5 days of VO_2 consumption, VCO_2 production (ml h^{-1}) and energy expenditure (kcal h^{-1}). Subsequently, each value was normalized per lean tissue mass extracted from the EchoMRI analysis.

Statistics and reproducibility

Statistical analyses were performed using Prism v.9.0 software, applying Mann–Whitney two-sided tests or one-way ANOVA for comparison (nonsignificant, $P > 0.05$; $^*P \le 0.05$; $^{**}P \le 0.01$; $^{***}P \le 0.001$; $^{****}P \le 0.0001$). P values are described in the figure legends and Source data tables. Significant statistical differences are indicated in the figures. More than three mice per condition and experiment were analysed as indicated in the figure legends and Source data tables. Immunofluorescence was performed more than once for each mouse with more than four paraffin or cryosections per mouse. The RNA sequencing experiment was performed once. pPCRs were performed using four to ten individual biological samples as indicated in figure legends; each biological sample was run in triplicate.

Reporting summary

Further information on research design is available in the Nature Portfolio Reporting Summary linked to this article.

Data availability

The mouse β-cell bulk RNA sequences generated in this study have been deposited in the NCBI GEO database (accession number GSE226479). All sequencing data were uploaded to and aligned on the Galaxy project80 against Ensembl reference genome GRCm38.p6 (release 100) (https://www.ensembl.org/Mus_musculus/Info/Index). The β-ID gene

list generated in a previous publication[79] (NCBI GEO database, accession number GSE150724) was used for analysis. The unfiltered list of differentially expressed genes is provided as Supplementary Data. Source data for Figs. 1–6 and Extended Data figures are provided with this paper in the Source data files; the availability of associated source data is indicated in each figure legend. Donor details for human samples are available in Supplementary Table 4. All data and materials used are available from commercial sources as presented in the Methods and from the corresponding author on reasonable request. Source data are provided with this paper.

References

1. Röder, P. V., Wu, B., Liu, Y. & Han, W. Pancreatic regulation of glucose homeostasis. *Exp. Mol. Med.* **48**, e219 (2016).
2. Svendsen, B. et al. Insulin secretion depends on intra-islet glucagon signaling. *Cell Rep.* **25**, 1127–1134.e2 (2018).
3. Capozzi, M. E., D'Alessio, D. A. & Campbell, J. E. The past, present, and future physiology and pharmacology of glucagon. *Cell Metab.* **34**, 1654–1674 (2022).
4. Huising, M. O. et al. CRFR1 is expressed on pancreatic β cells, promotes β cell proliferation, and potentiates insulin secretion in a glucose-dependent manner. *Proc. Natl Acad. Sci. USA* **107**, 912–917 (2010).
5. Rodriguez-Diaz, R. et al. Alpha cells secrete acetylcholine as a non-neuronal paracrine signal priming beta cell function in humans. *Nat. Med.* **17**, 888–892 (2011).
6. Strowski, M. Z., Parmar, R. M., Blake, A. D. & Schaeffer, J. M. Somatostatin inhibits insulin and glucagon secretion via two receptors subtypes: an in vitro study of pancreatic islets from somatostatin receptor 2 knockout mice. *Endocrinology* **141**, 111–117 (2000).
7. Aragón, F. et al. Pancreatic polypeptide regulates glucagon release through PPYR1 receptors expressed in mouse and human alpha-cells. *Biochim. Biophys. Acta* **1850**, 343–351 (2015).
8. Khan, D., Vasu, S., Moffett, R. C., Irwin, N. & Flatt, P. R. Influence of neuropeptide Y and pancreatic polypeptide on islet function and beta-cell survival. *Biochim. Biophys. Acta* **1861**, 749–758 (2017).
9. Thorel, F. et al. Conversion of adult pancreatic α-cells to β-cells after extreme β-cell loss. *Nature* **464**, 1149–1154 (2010).
10. Chera, S. et al. Diabetes recovery by age-dependent conversion of pancreatic δ-cells into insulin producers. *Nature* **514**, 503–507 (2014).
11. Damond, N. et al. Blockade of glucagon signaling prevents or reverses diabetes onset only if residual β-cells persist. *eLife* **5**, e13828 (2016).
12. Cigliola, V. et al. Pancreatic islet-autonomous insulin and smoothened-mediated signalling modulate identity changes of glucagon$^+$ α-cells. *Nat. Cell Biol.* **20**, 1267–1277 (2018).
13. Furuyama, K. et al. Diabetes relief in mice by glucose-sensing insulin-secreting human α-cells. *Nature* **567**, 43–48 (2019).
14. Perez-Frances, M. et al. Pancreatic Ppy-expressing γ-cells display mixed phenotypic traits and the adaptive plasticity to engage insulin production. *Nat. Commun.* **12**, 4458 (2021).
15. Thorel, F. et al. Normal glucagon signaling and β-cell function after near-total α-cell ablation in adult mice. *Diabetes* **60**, 2872–2882 (2011).
16. Kumar, U. & Singh, S. Role of somatostatin in the regulation of central and peripheral factors of satiety and obesity. *Int. J. Mol. Sci.* **21**, 2568 (2020).
17. Lukomska, A., Dobrzanski, G., Liguz-Lecznar, M. & Kossut, M. Somatostatin receptors (SSTR1-5) on inhibitory interneurons in the barrel cortex. *Brain Struct. Funct.* **225**, 387–401 (2020).
18. Scheggia, D. et al. Somatostatin interneurons in the prefrontal cortex control affective state discrimination in mice. *Nat. Neurosci.* **23**, 47–60 (2020).
19. Urban-Ciecko, J. & Barth, A. L. Somatostatin-expressing neurons in cortical networks. *Nat. Rev. Neurosci.* **17**, 401–409 (2016).
20. Traub, S. et al. Pancreatic α cell-derived glucagon-related peptides are required for β cell adaptation and glucose homeostasis. *Cell Rep.* **18**, 3192–3203 (2017).
21. Tellez, K. et al. In vivo studies of glucagon secretion by human islets transplanted in mice. *Nat. Metab.* **2**, 547–557 (2020).
22. Marciniak, A. et al. Using pancreas tissue slices for in situ studies of islet of Langerhans and acinar cell biology. *Nat. Protoc.* **9**, 2809–2822 (2014).
23. Wortley, K. E. et al. Peptide YY regulates bone turnover in rodents. *Gastroenterology* **133**, 1534–1543 (2007).
24. Huang, J. L. et al. Paracrine signalling by pancreatic δ cells determines the glycaemic set point in mice. *Nat. Metab.* **6**, 61–77 (2024).
25. Hauge-Evans, A. C. et al. Somatostatin secreted by islet δ-cells fulfills multiple roles as a paracrine regulator of islet function. *Diabetes* **58**, 403–411 (2009).
26. Zhang, J., McKenna, L. B., Bogue, C. W. & Kaestner, K. H. The diabetes gene *Hhex* maintains δ-cell differentiation and islet function. *Genes Dev.* **28**, 829–834 (2014).
27. Yabe, D. & Seino, Y. Two incretin hormones GLP-1 and GIP: comparison of their actions in insulin secretion and β cell preservation. *Prog. Biophys. Mol. Biol.* **107**, 248–256 (2011).
28. Kjems, L. L., Holst, J. J., Vølund, A. & Madsbad, S. The influence of GLP-1 on glucose-stimulated insulin secretion: effects on β-cell sensitivity in type 2 and nondiabetic subjects. *Diabetes* **52**, 380–386 (2003).
29. MacDonald, P. E. et al. The multiple actions of GLP-1 on the process of glucose-stimulated insulin secretion. *Diabetes* **51**, S434–S442 (2002).
30. Holst, J. J. The physiology of glucagon-like peptide 1. *Physiol. Rev.* **87**, 1409–1439 (2007).
31. Holter, M. M., Saikia, M. & Cummings, B. P. Alpha-cell paracrine signaling in the regulation of beta-cell insulin secretion. *Front. Endocrinol* **13**, 934775 (2022).
32. Zhang, F. et al. Recombinant human GLP-1 beinaglutide regulates lipid metabolism of adipose tissues in diet-induced obese mice. *iScience* **24**, 103382 (2021).
33. Liu, F. et al. The effects of glucagon-like peptide-1 receptor agonists on adipose tissues in patients with type 2 diabetes: a meta-analysis of randomised controlled trials. *PLoS ONE* **17**, e0270899 (2022).
34. Jiang, Y. et al. GLP-1 improves adipocyte insulin sensitivity following induction of endoplasmic reticulum stress. *Front. Pharmacol.* **9**, 1168 (2018).
35. Wu, H. et al. The GLP-1 analogue exenatide improves hepatic and muscle insulin sensitivity in diabetic rats: tracer studies in the basal state and during hyperinsulinemic–euglycemic clamp. *J. Diabetes Res.* **2014**, 524517 (2014).
36. Qin, Y. et al. Liraglutide improves hepatic insulin resistance via the canonical Wnt signaling pathway. *Mol. Med. Rep.* **17**, 7372–7380 (2018).
37. de Souza, A. H. et al. Intra-islet GLP-1, but not CCK, is necessary for β-cell function in mouse and human islets. *Sci. Rep.* **10**, 2823 (2020).
38. Hodson, D. J. et al. Lipotoxicity disrupts incretin-regulated human β cell connectivity. *J. Clin. Invest.* **123**, 4182–4194 (2013).
39. Miranda, C., Begum, M., Vergari, E. & Briant, L. J. B. Gap junction coupling and islet delta-cell function in health and disease. *Peptides* **147**, 170704 (2022).
40. Briant, L. J. B. et al. δ-cells and β-cells are electrically coupled and regulate α-cell activity via somatostatin. *J. Physiol.* **596**, 197–215 (2018).
41. Meda, P. Gap junction proteins are key drivers of endocrine function. *Biochim. Biophys. Acta* **1860**, 124–140 (2018).

42. Lei, C. L. et al. Beta-cell hubs maintain Ca^{2+} oscillations in human and mouse islet simulations. *Islets* **10**, 151–167 (2018).
43. Satin, L. S., Zhang, Q. & Rorsman, P. 'Take me to your leader': an electrophysiological appraisal of the role of hub cells in pancreatic islets. *Diabetes* **69**, 830–836 (2020).
44. Ravier, M. A. et al. Loss of connexin36 channels alters β-cell coupling, islet synchronization of glucose-induced Ca^{2+} and insulin oscillations, and basal insulin release. *Diabetes* **54**, 1798–1807 (2005).
45. Seemann, N., Welling, A. & Rustenbeck, I. The inhibitor of connexin Cx36 channels, mefloquine, inhibits voltage-dependent Ca^{2+} channels and insulin secretion. *Mol. Cell. Endocrinol.* **472**, 97–106 (2018).
46. Pipeleers, D. G. et al. Interplay of nutrients and hormones in the regulation of insulin release. *Endocrinology* **117**, 824–833 (1985).
47. Steiner, D. J., Kim, A., Miller, K. & Hara, M. Pancreatic islet plasticity: interspecies comparison of islet architecture and composition. *Islets* **2**, 135–145 (2010).
48. Cabrera, O. et al. The unique cytoarchitecture of human pancreatic islets has implications for islet cell function. *Proc. Natl Acad. Sci. USA* **103**, 2334–2339 (2006).
49. Bosco, D. et al. Unique arrangement of α- and β-cells in human islets of Langerhans. *Diabetes* **59**, 1202–1210 (2010).
50. Dolenšek, J., Rupnik, M. S. & Stožer, A. Structural similarities and differences between the human and the mouse pancreas. *Islets* **7**, e1024405 (2015).
51. Blum, B. et al. Functional beta-cell maturation is marked by an increased glucose threshold and by expression of urocortin 3. *Nat. Biotechnol.* **30**, 261–264 (2012).
52. van der Meulen, T. et al. Urocortin3 mediates somatostatin-dependent negative feedback control of insulin secretion. *Nat. Med.* **21**, 769–776 (2015).
53. Li, N. et al. Ablation of somatostatin cells leads to impaired pancreatic islet function and neonatal death in rodents. *Cell Death Dis.* **9**, 682 (2018).
54. Huang, J. L. et al. Genetic deletion of Urocortin 3 does not prevent functional maturation of beta cells. *J. Endocrinol.* **246**, 69–78 (2020).
55. Herrera, P. L. et al. Ablation of islet endocrine cells by targeted expression of hormone-promoter-driven toxigenes. *Proc. Natl Acad. Sci. USA* **91**, 12999–13003 (1994).
56. Perez-Frances, M. et al. Adult pancreatic islet endocrine cells emerge as fetal hormone-expressing cells. *Cell Rep.* **38**, 110377 (2022).
57. Vuguin, P. M. et al. Ablation of the glucagon receptor gene increases fetal lethality and produces alterations in islet development and maturation. *Endocrinology* **147**, 3995–4006 (2006).
58. Cho, Y. M., Merchant, C. E. & Kieffer, T. J. Targeting the glucagon receptor family for diabetes and obesity therapy. *Pharmacol. Ther.* **135**, 247–278 (2012).
59. Wang, M. Y. et al. Glucagon receptor antibody completely suppresses type 1 diabetes phenotype without insulin by disrupting a novel diabetogenic pathway. *Proc. Natl Acad. Sci. USA* **112**, 2503–2508 (2015).
60. Klempel, N., Thomas, K., Conlon, J. M., Flatt, P. R. & Irwin, N. Alpha-cells and therapy of diabetes: Inhibition, antagonism or death? *Peptides* **157**, 170877 (2022).
61. Brissova, M. et al. α Cell function and gene expression are compromised in type 1 diabetes. *Cell Rep.* **22**, 2667–2676 (2018).
62. Doliba, N. M. et al. α Cell dysfunction in islets from nondiabetic, glutamic acid decarboxylase autoantibody-positive individuals. *J. Clin. Invest.* **132**, e156243 (2022).
63. Bosi, E., Marchetti, P., Rutter, G. A. & Eizirik, D. L. Human alpha cell transcriptomic signatures of types 1 and 2 diabetes highlight disease-specific dysfunction pathways. *iScience* **25**, 105056 (2022).
64. Brown, R. J., Sinaii, N. & Rother, K. I. Too much glucagon, too little insulin: time course of pancreatic islet dysfunction in new-onset type 1 diabetes. *Diabetes Care* **31**, 1403–1404 (2008).
65. Kramer, C. K., Borgoño, C. A., Van Nostrand, P., Retnakaran, R. & Zinman, B. Glucagon response to oral glucose challenge in type 1 diabetes: lack of impact of euglycemia. *Diabetes Care* **37**, 1076–1082 (2014).
66. Shah, P. et al. Lack of suppression of glucagon contributes to postprandial hyperglycemia in subjects with type 2 diabetes mellitus. *J. Clin. Endocrinol. Metab.* **85**, 4053–4059 (2000).
67. Petersen, K. F. & Sullivan, J. T. Effects of a novel glucagon receptor antagonist (Bay 27-9955) on glucagon-stimulated glucose production in humans. *Diabetologia* **44**, 2018–2024 (2001).
68. Bengtsen, M. B. et al. A human randomized controlled trial comparing metabolic responses to single and repeated hypoglycemia in type 1 diabetes. *J. Clin. Endocrinol. Metab.* **105**, e4699–e4711 (2020).
69. Siafarikas, A. et al. Early loss of the glucagon response to hypoglycemia in adolescents with type 1 diabetes. *Diabetes Care* **35**, 1757–1762 (2012).
70. Yue, J. T. et al. Somatostatin receptor type 2 antagonism improves glucagon and corticosterone counterregulatory responses to hypoglycemia in streptozotocin-induced diabetic rats. *Diabetes* **61**, 197–207 (2012).
71. Karimian, N. et al. Somatostatin receptor type 2 antagonism improves glucagon counterregulation in biobreeding diabetic rats. *Diabetes* **62**, 2968–2977 (2013).
72. Arrojo, E. D. R. et al. Structural basis for delta cell paracrine regulation in pancreatic islets. *Nat. Commun.* **10**, 3700 (2019).
73. Rorsman, P. & Huising, M. O. The somatostatin-secreting pancreatic δ-cell in health and disease. *Nat. Rev. Endocrinol.* **14**, 404–414 (2018).
74. Oropeza, D. & Herrera, P. L. Glucagon-producing α-cell transcriptional identity and reprogramming towards insulin production. *Trends Cell Biol.* **34**, 180–197 (2024).
75. Wang, X., Gao, M., Wang, Y. & Zhang, Y. The progress of pluripotent stem cell-derived pancreatic β-cells regeneration for diabetic therapy. *Front. Endocrinol.* **13**, 927324 (2022).
76. Pagliuca, F. W. & Melton, D. A. How to make a functional β-cell. *Development* **140**, 2472–2483 (2013).
77. Cigliola, V., Ghila, L., Chera, S. & Herrera, P. L. Tissue repair brakes: a common paradigm in the biology of regeneration. *Stem Cells* **38**, 330–339 (2020).
78. Chera, S. & Herrera, P. L. Regeneration of pancreatic insulin-producing cells by in situ adaptive cell conversion. *Curr. Opin. Genet. Dev.* **40**, 1–10 (2016).
79. van Gurp, L. et al. Generation of human islet cell type-specific identity genesets. *Nat. Commun.* **13**, 2020 (2022).
80. Afgan, E. et al. The Galaxy platform for accessible, reproducible and collaborative biomedical analyses: 2016 update. *Nucleic Acids Res.* **44**, W3–W10 (2016).
81. Dobin, A. et al. STAR: ultrafast universal RNA-seq aligner. *Bioinformatics* **29**, 15–21 (2013).
82. Anders, S., Pyl, P. T. & Huber, W. HTSeq—a Python framework to work with high-throughput sequencing data. *Bioinformatics* **31**, 166–169 (2015).
83. Love, M. I., Huber, W. & Anders, S. Moderated estimation of fold change and dispersion for RNA-seq data with DESeq2. *Genome Biol.* **15**, 550 (2014).

84. Anderson, J. G. et al. Enhanced insulin sensitivity in skeletal muscle and liver by physiological overexpression of SIRT6. *Mol. Metab.* **4**, 846–856 (2015).
85. Cohrs, C. M. et al. Vessel network architecture of adult human islets promotes distinct cell–cell interactions in situ and is altered after transplantation. *Endocrinology* **158**, 1373–1385 (2017).
86. Taddeo, E. P. et al. Individual islet respirometry reveals functional diversity within the islet population of mice and human donors. *Mol. Metab.* **16**, 150–159 (2018).

Acknowledgements

We thank G. Gallardo, C. Gysler and B. Polat for technical help, S. Chera for the scientific discussions, J.-P. Aubry-Lachainaye and G. Schneiter for FACS assistance, M. Docquier for RNA sequencing advice and C. Veyrat-Durebex and F. Bontems for physiological and metabolic advice and support. Human pancreatic islets isolated from deceased (brain-dead) multiorgan donors were obtained from three different centres: (1) the NIDDK-funded integrated Islet Distribution Program (IIDP) at City of Hope (RRID: SCR_014387), National Institutes of Health grant no. 2UC4DK098085; (2) the Alberta Diabetes Institute IsletCore at the University of Alberta in Edmonton (http://www.bcell.org/adi-isletcore.html) with the assistance of the Human Organ Procurement and Exchange (HOPE) program, Trillium Gift of Life Network (TGLN) and other Canadian organ procurement organizations (islet isolation was approved by the Human Research Ethics Board at the University of Alberta (Pro00013094)); and (3) the Geneva University Hospital (CCER protocol 2016-01979; Laboratoire d'Isolement et de Transplantation Cellulaires, Dépt. de Chirugie), with approved islet use according to CCER protocol 2019-00518. This work was funded with grants from the Swiss National Science Foundation (nos. 310030_192496, 310030E_205640 and 320030_227816), the European Research Council (no. 884449; 'Merlin' Advanced Grant) and the Fondation Aclon to P.L.H., and the JST FOREST Program (#JPMJFR210Y) to K.F. The funders had no role in study design, data collection and analysis, decision to publish or preparation of the manuscript.

Author contributions

M.P.F. conceived and performed the experiments and analyses and wrote the paper. E.B.T. conceived and performed the human islet experiments and analysis and wrote the paper. C.C. and S.S. performed the dynamic insulin secretion experiments. M.V.A. developed and bred the non-β-DTR mouse line. L.v.G. analysed the transcriptomic data. K.F. conceived the human islet experiments. F.T. and P.L.H. generated the non-β-DTR mouse line, conceived the experiments, interpreted the observations and wrote the paper.

Competing interests

The authors declare no competing interests.

Additional information

Extended data is available for this paper at https://doi.org/10.1038/s42255-024-01114-8.

Supplementary information The online version contains supplementary material available at https://doi.org/10.1038/s42255-024-01114-8.

Correspondence and requests for materials should be addressed to Pedro L. Herrera.

Peer review information *Nature Metabolism* thanks Gordon Weir and the other, anonymous, reviewer(s) for their contribution to the peer review of this work. Primary Handling Editors: Revati Dewal and Isabella Samuelson, in collaboration with the *Nature Metabolism* team.

Reprints and permissions information is available at www.nature.com/reprints.

Publisher's note Springer Nature remains neutral with regard to jurisdictional claims in published maps and institutional affiliations.

Open Access This article is licensed under a Creative Commons Attribution-NonCommercial-NoDerivatives 4.0 International License, which permits any non-commercial use, sharing, distribution and reproduction in any medium or format, as long as you give appropriate credit to the original author(s) and the source, provide a link to the Creative Commons licence, and indicate if you modified the licensed material. You do not have permission under this licence to share adapted material derived from this article or parts of it. The images or other third party material in this article are included in the article's Creative Commons licence, unless indicated otherwise in a credit line to the material. If material is not included in the article's Creative Commons licence and your intended use is not permitted by statutory regulation or exceeds the permitted use, you will need to obtain permission directly from the copyright holder. To view a copy of this licence, visit http://creativecommons.org/licenses/by-nc-nd/4.0/.

© The Author(s) 2024

https://doi.org/10.1038/s42255-024-01114-8

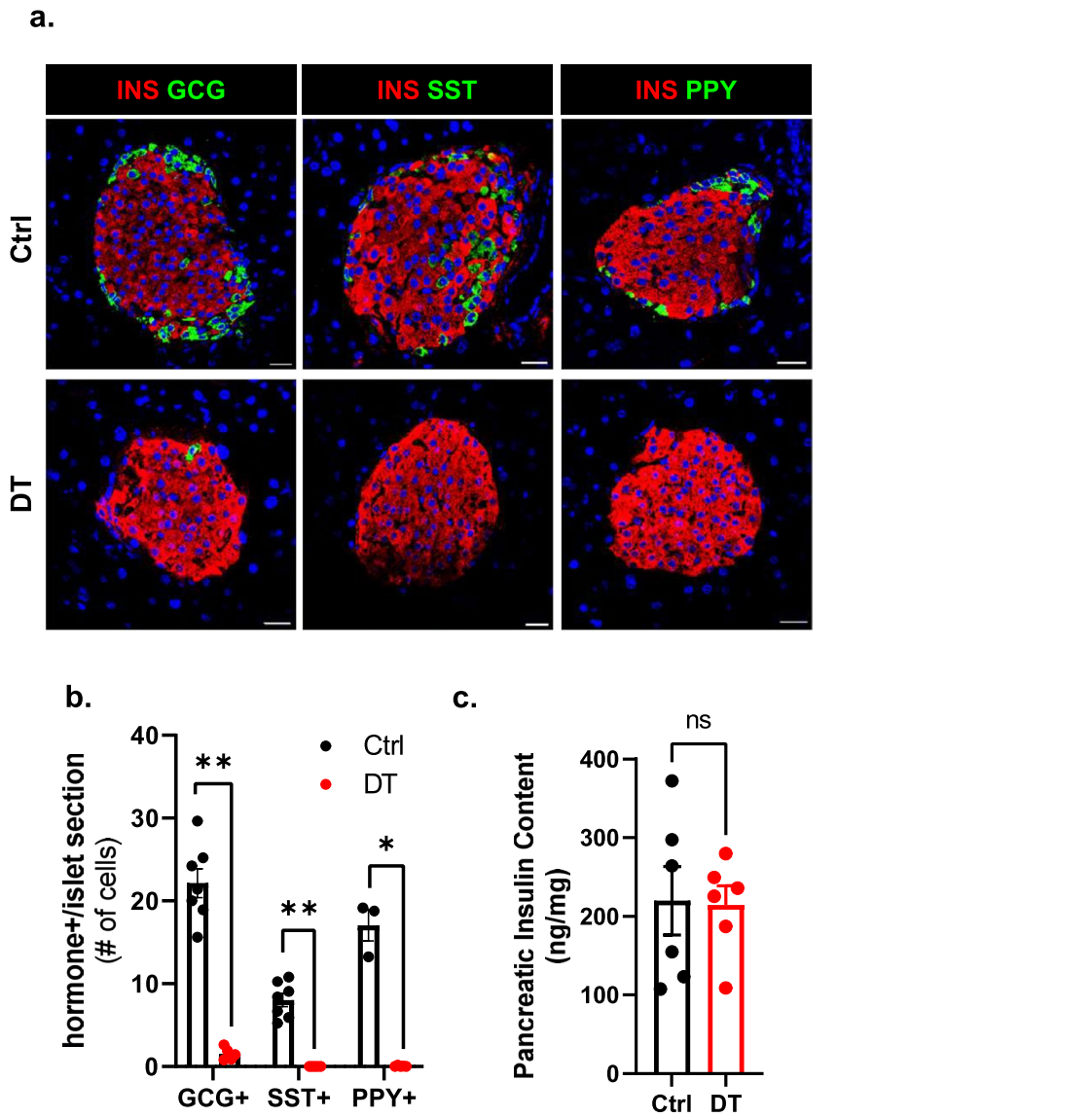

Extended Data Fig. 1 | Long-term characterization of aged mice 40-weeks after non-β-cell ablation. a. Immunofluorescence on pancreas tissue sections from control (Ctrl) or DT-treated mice analyzed 40 weeks post-ablation (wpa). INS: red; GCG: green (left); INS: red; SST: green (middle); INS: red; PPY: green (right). Scale bar: 20 µm. **b**. Quantification of GCG+, SST+, and PPY+ cells in Ctrl (black) or DT (red) mice 40wpa. GCG+ and SST+ (Ctrl n = 7, DT n = 5) cells were scored in the dorsal region of the pancreas; PPY+ (Ctrl n = 3, DT n = 5) cells were scored in the ventral region of the pancreas. P-values Ctrl vs DT: GCG + P = 0.0025, SST + P = 0.0025, PPY + P = 0.036. **c**. Pancreatic insulin content (ng/mg) of Ctrl (black, n = 6) and DT (red, n = 6) mice 40wpa. P-value Ctrl vs DT = 0.937. Only male mice were used. All data are shown as mean ± sem. All statistical tests are two-tailed Mann-Whitney test. Source data is available.

https://doi.org/10.1038/s42255-024-01114-8

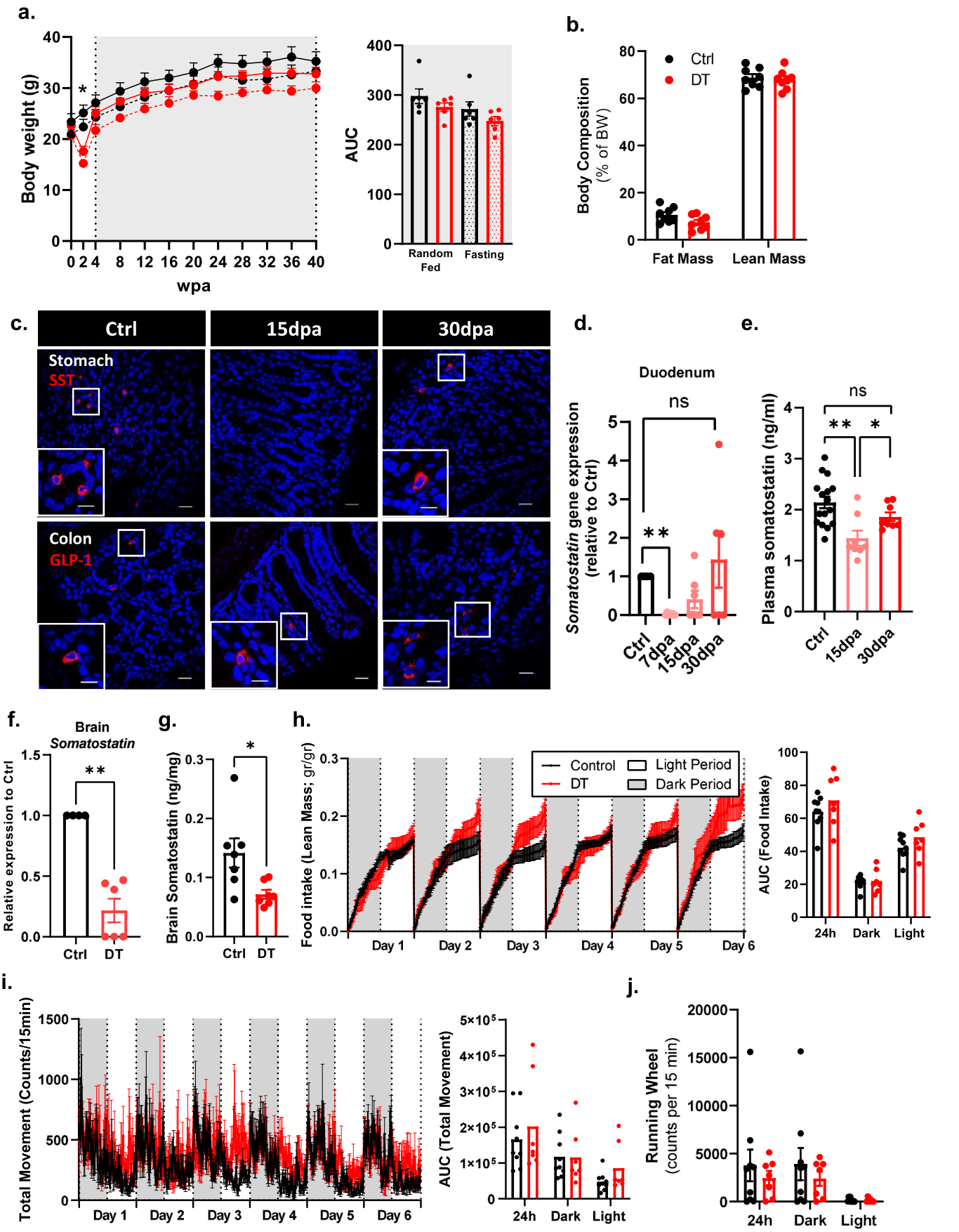

Extended Data Fig. 2 | See next page for caption.

https://doi.org/10.1038/s42255-024-01114-8

Extended Data Fig. 2 | Somatostatin-producing intestinal D-cell ablation and regeneration in β-only mice. a, Body weight over 40weeks on Ctrl (black, n = 6) and DT (red, n = 6) mice in random fed (RF, continuous line) and fasting (F, dashed line). Right panel: Area under the curve (AUC). P-values (DTvsCtrl): RF P = 0.3312, F P = 0.3939. **b**, Body composition in Ctrl (black, n = 8) and DT (red, n = 8) mice. P-values CtrlvsDT: Lean mass P = 0.7209, Fat mass P = 0.083. **c**, Immunofluorescence on SST (red) in stomach (upper micrographs) and GLP-1 (red) in colon (lower micrographs) from Ctrl or β-only mice. Scale bar: 20 µm or 10 µm (insets). **d**, Duodenum qPCR of Sst of Ctrl (black, n = 4) and β-only mice at 7 dpa (pink, n = 7), 15 dpa (light red, n = 7), and 30 dpa (red, n = 6). Data are normalized ct values relative to β-actin and Gapdh and shown as relative hormone expression to Ctrl. P-values: 7 dpa vs Ctrl P = 0.0061, 15 dpa vs Ctrl P = 0.0606, 30 dpa vs Ctrl P = > 0.999. **e**, Plasma somatostatin in Ctrl (n = 16) and β-only after 15 dpa (pink, n = 8) and 30 dpa (red, n = 8). P-values: 15 dpa vs Ctrl P = 0.0016, 30 dpa vs Ctrl P = 0.1090, 30 dpa vs 15 dpa P = 0.0468. **f**, Brain qPCR on Sst of Ctrl (black, n = 4) and β-only (red, n = 6). Data are normalized ct values relative to β-actin and Gapdh and shown as relative hormone expression to Ctrl. P-values Ctrl vs DT: P = 0.0095. **g**, Brain somatostatin of Ctrl (n = 8) and β-only (n = 7). P-values: DT vs Ctrl P = 0.0128. **h**-**j**, Food intake (h; gr/gr), total movement (i; counts, infrared breaks in 15 minutes) and running wheel activity (j) in Ctrl (black, n = 9) and DT (red, n = 7). Right panel: AUC. Food intake (h) P-value (CtrlvsDT): light period P = 0.2523; dark period P = 0.6065; 24 h P = 0.4079. Total movement (i) P-value (CtrlvsDT): light period P = 0.2105; dark period P = 0.8371; 24 h period P = 0.7577. Running wheel (j) P-value (CtrlvsDT): light period P = > 0.99; dark period P = 0.9182; 24 h period P = > 0.99. Only male mice were used. All data are shown as mean ± sem. All statistical tests are two-tailed Mann-Whitney test. Source data is available.

https://doi.org/10.1038/s42255-024-01114-8

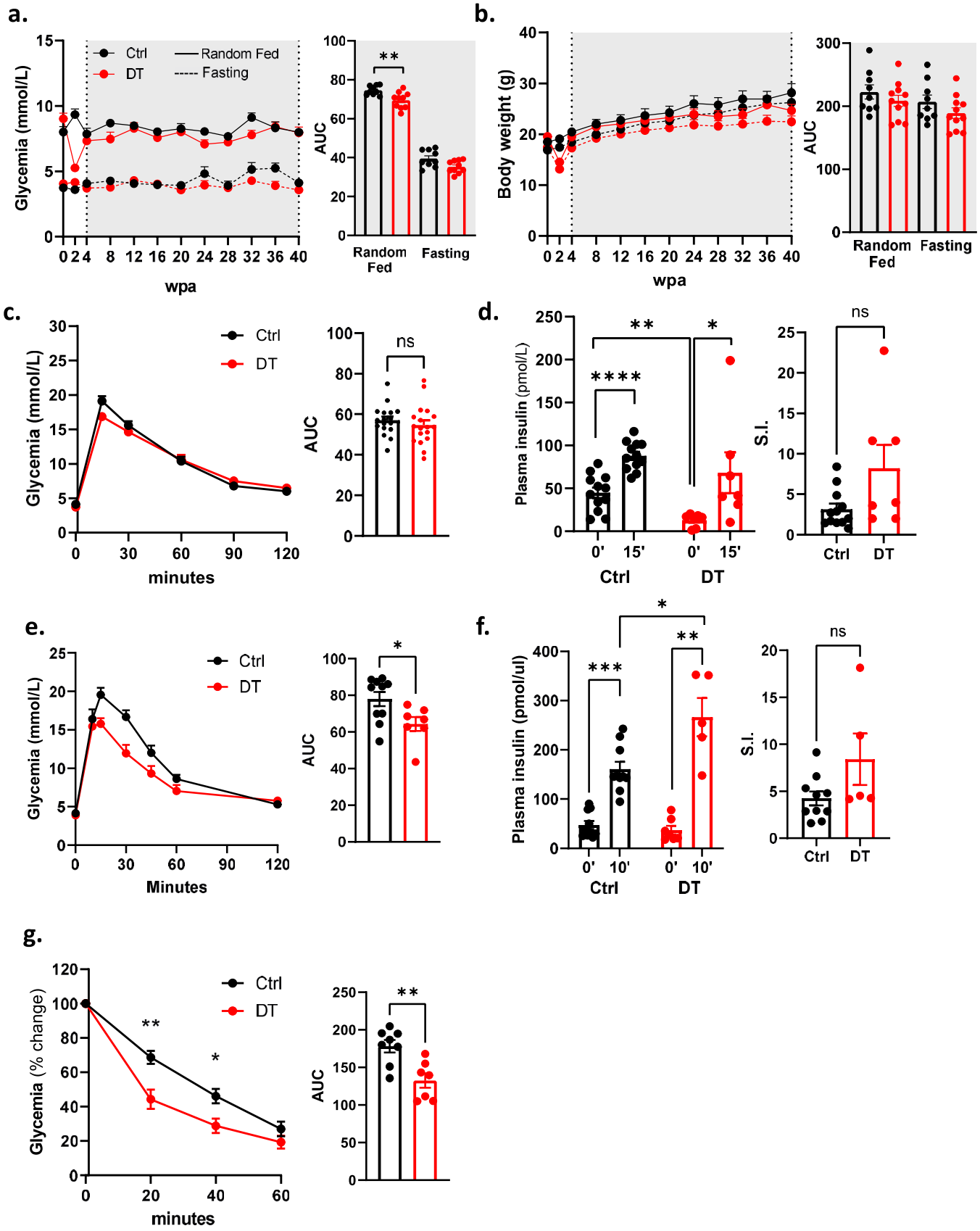

Extended Data Fig. 3 | See next page for caption.

https://doi.org/10.1038/s42255-024-01114-8

Extended Data Fig. 3 | Improved blood glucose homeostasis in female β-only mice. a. Glycemia over 40 weeks post-ablation of Ctrl (black; n = 9) and DT (red; n = 10) female mice in random-fed (RF, continuous line) or fasting (F, dashed line). Right panel: area under the curve (AUC) of glycemia. P-values (DT vs Ctrl): RF P = 0.0038; F P = 0.067. **b**. Body weight over 40 weeks post-ablation of Ctrl (black; n = 9) and DT (red; n = 10) female mice in RF (continuous line) or F (dashed line). Right panel: AUC of body weight. P-values DT vs Ctrl: RF P = 0.468; F P = 0.2013. **c**. Intraperitoneal glucose tolerance test (ipGTT) at 4wpa. Left panel: ipGTT on Ctrl (black; n = 17) and DT (red; n = 18). Right panel: AUC of ipGTT; P-value (Ctrl vs DT) P = 0.3142. **d**. Plasma insulin along ipGTT. Left panel: plasma insulin at 0 and 15 minutes after glucose injection in Ctrl (black; n = 12) and DT (red; n = 7) mice. Right panel: stimulation index (S.I.) of insulin secretion. P-value (Ctrl vs DT) P = 0.0646. **e**. Oral glucose tolerance test (oGTT) at 30 dpa. Left panel: oGTT on Ctrl (black; n = 10) and DT (red; n = 7). Right panel: AUC of oGTT. P-value (Ctrl vs DT) = 0.0431. **f**. Plasma insulin along oGTT. Left panel: plasma insulin at 0 and 10 minutes after glucose gavage in Ctrl (black; n = 10) and DT (red; n = 6) mice. Right panel: stimulation index (S.I.) of insulin secretion. P-value Ctrl vs DT P = 0.2424. **g**. Insulin tolerance test (ITT) at 30 dpa. Left panel: ITT on Ctrl (black; n = 8) and DT (red; n = 7) mice. Data are shown as % relative to glycemia at time 0. Right panel: AUC of ITT. P-value Ctrl vs DT P = 0.0093. Error bars denote s.e.m. Two-tailed Mann-Whitney test. Source data is available.

https://doi.org/10.1038/s42255-024-01114-8

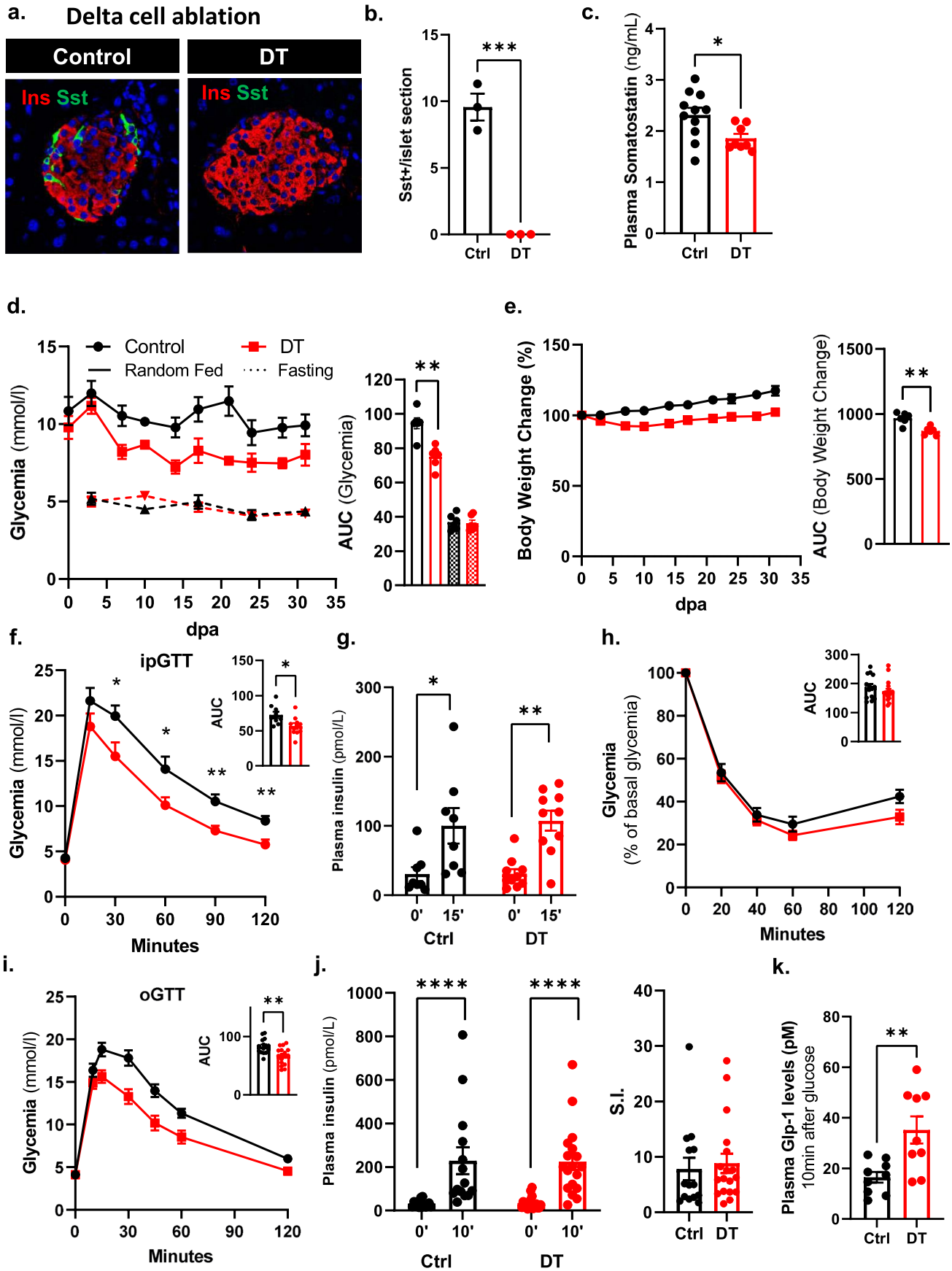

Extended Data Fig. 4 | See next page for caption.

https://doi.org/10.1038/s42255-024-01114-8

Extended Data Fig. 4 | Blood glucose homeostasis in mice without somatostatin-expressing δ-cells. a, Pancreas immunofluorescence from control (Ctrl) or δ-cell ablated mice. INS: red; SST: green. Scale bars: 20 µm. **b**. Quantification of SST+ cells per islet section in Ctrl (black, n = 3) or DT (red, n = 3) mice (dorsal pancreas). P-values CtrlvsDT P = 0.0007. **c**, Plasma somatostatin (ng/ml) in Ctrl (black, n = 11) and DT (red, n = 8). P-values CtrlvsDT: P = 0.0157. **d**, Glycemia of Ctrl (black, n = 6) and DT (red, n = 6) in RF (continuous line) or F (dashed line). Right panel: area under the curve (AUC). P-values: RF DTvsCtrl P = 0.0043; F DTvsCtrl P = 0.8182. **e**, Body weight change (% from day 0) of Ctrl (black, n = 6) and DT (red, n = 6) in random-fed. Right panel: AUC. P-values: RF DTvsCtrl P = 0.0043. **f**, Intraperitoneal glucose tolerance test (ipGTT) on Ctrl (black, n = 9) and DT (red, n = 10). Right panel: AUC; P-value CtrlvsDT P = 0.0279. **g**, Plasma insulin at 0 and 15 minutes after glucose in Ctrl (black, n = 8) and DT (red, n = 10). P-value Ctrl (0′ vs 15′) = 0.0140; DT (0′ vs 15′) = 0.0015. **h**, Insulin tolerance test (ITT) on Ctrl (black, n = 9) and DT (red, n = 10). Data are shown as % relative to glycemia at time 0. Right panel: AUC; P-value CtrlvsDT=0.0789. **i**, Oral glucose tolerance test (oGTT) on Ctrl (black, n = 8) and DT (red, n = 10). Right panel: AUC; P-value (CtrlvsDT) = 0.0055. **j**, Plasma insulin at 0 and 10 minutes after glucose in Ctrl (black, n = 7) and DT (red, n = 10). P-value Ctrl (0′ vs 10′) = 0.0041; DT (0′ vs 10′) = 0.0011. Right panel: stimulation index (S.I.) of insulin; P-value (CtrlvsDT)=0.9623. **k**, Plasma GLP-1 along oGTT in Ctrl (black, n = 9) and DT (red, n = 9). P-value (CtrlvsDT)=0.0056. Only male mice were used. Data are shown as mean ± sem. Statistical tests are two-tailed Mann-Whitney. Source data is available.

https://doi.org/10.1038/s42255-024-01114-8

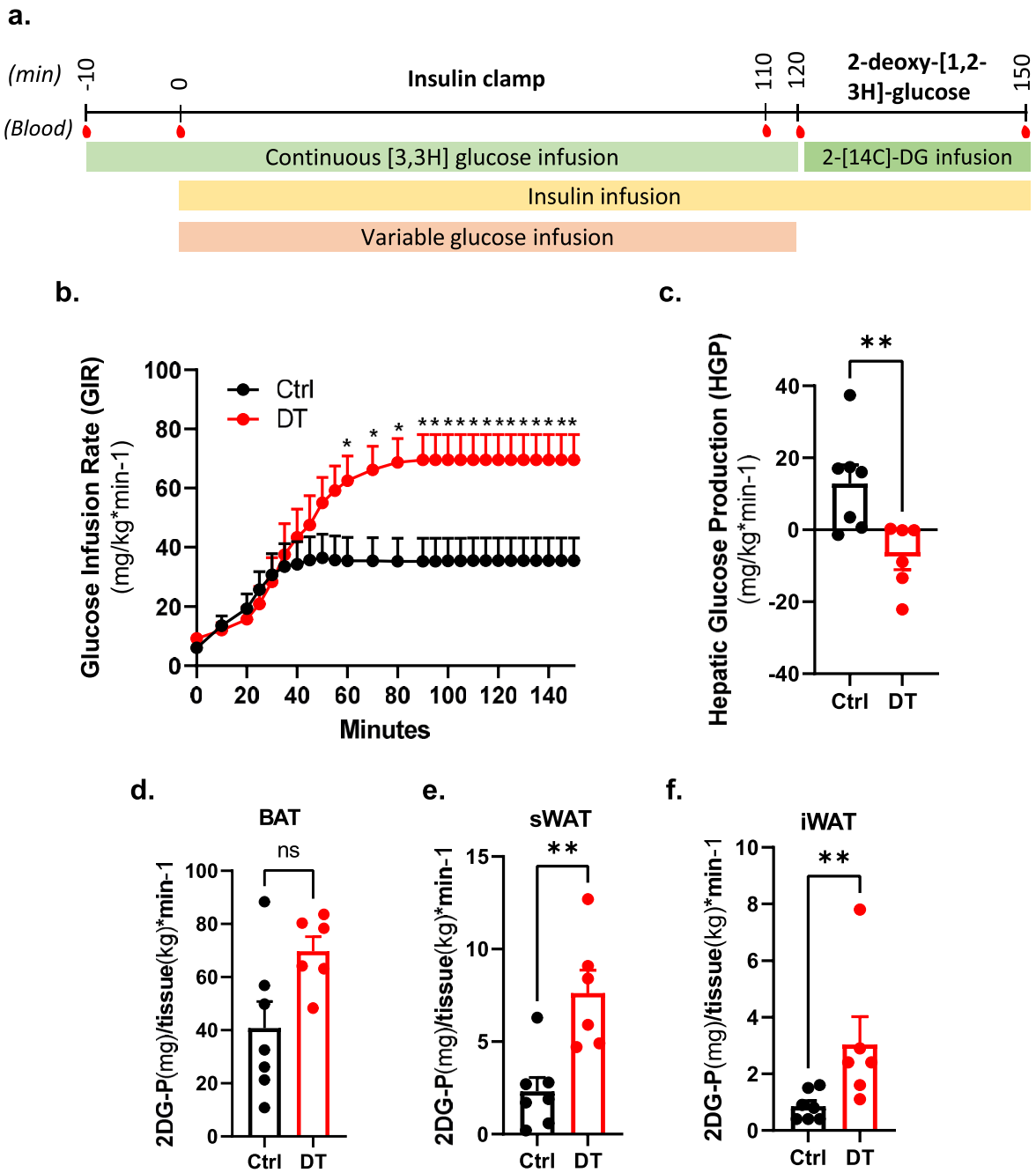

Extended Data Fig. 5 | Hyperinsulinemic-euglycemic clamp after non β-cell ablation. a, Experimental time-line for the hyperinsulinemic-euglycemic clamp. 2.5mUI/kg/min of insulin were continuously infused during the insulin clamp. Blood samples were taken at multiple time for further analyses. **b-c**, Glucose infusion rate (GIR, b) and hepatic glucose production (HGP, c) measured during clamp studies in Ctrl (black, n = 7) and DT (red, n = 6) mice. P-values: CtrlvsDT HGP P = 0.007. **d-f**, Radiolabeled 2-deoxy-D-glucose (2DG) uptake by adipose tissue in Ctrl (black, n = 7) and DT (red, n = 6) mice. P-values (Ctrl vs DT): Brown Adipose Tissue (BAT) P = 0.073; subcutaneous White Adipose Tissue (sWAT) P = 0.008; inguinal White Adipose Tissue (iWAT) P = 0.005. Insulin clamp and 2DG uptake were obtained from the same mice. Only male mice were used. All data are shown as mean ± sem. All statistical tests are two-tailed Mann-Whitney test. Source data is available.

https://doi.org/10.1038/s42255-024-01114-8

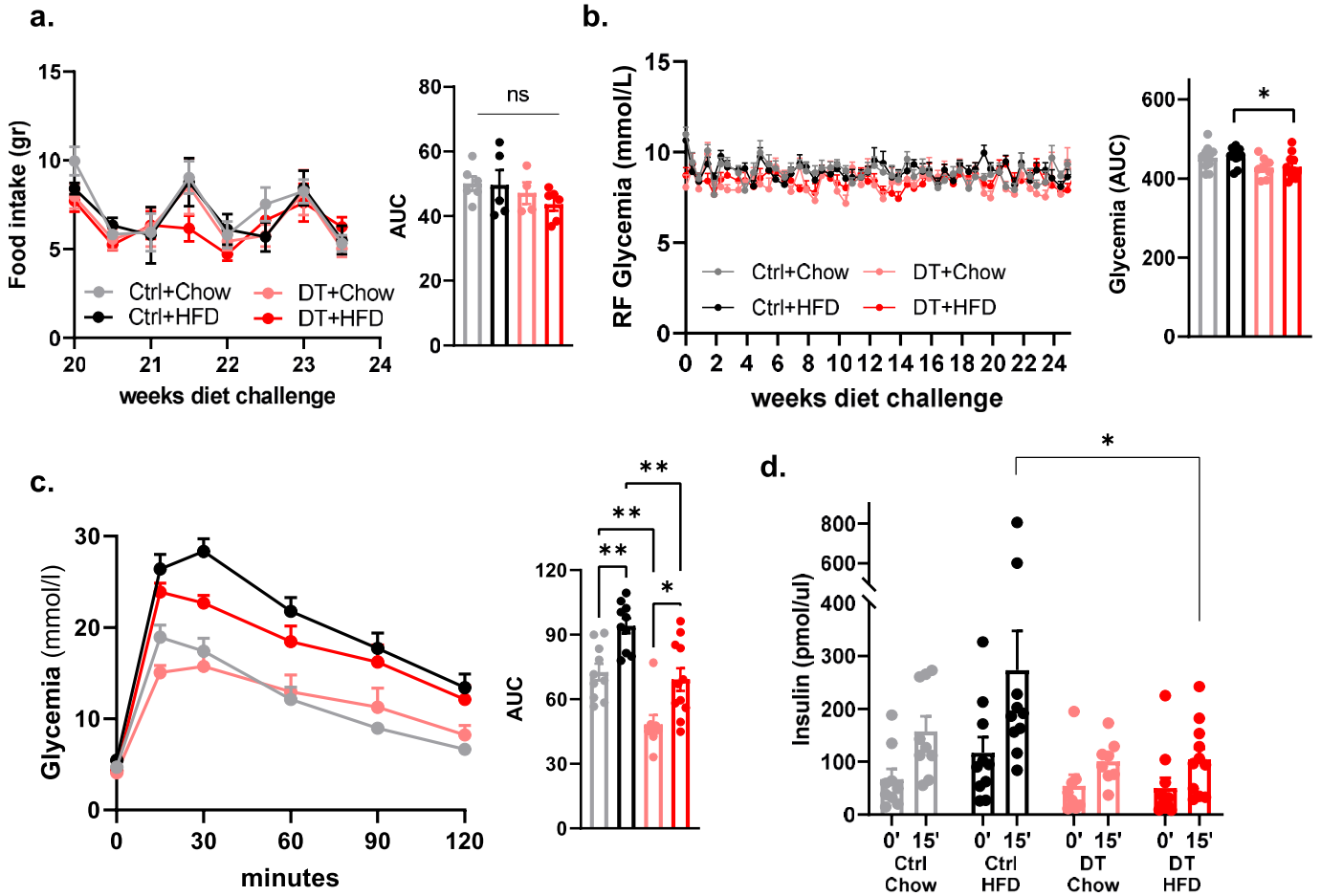

Extended Data Fig. 6 | High-fat diet administration to β-only mice. a, Food intake (gr) of Ctrl+Chow (grey, n = 6), Ctrl+HFD (black, n = 5), DT+Chow (pink, n = 4), DT + HFD (red, n = 6) over the last 4-weeks of high-fat diet (HFD). Right panel: area under the curve (AUC). P-values: Ctrl+chow vs Ctrl+HFD P = 0.7922, Ctrl+chow vs DT+chow P = 0.4762, Ctrl+chow vs DT + HFD P = 0.0649, Ctrl+HFD vs DT+chow P = 0.9048, Ctrl+HFD vs DT + HFD P = 0.6623; DT+chow vs DT + HFD P = 0.4762. **b**, Random fed glycemia of Ctrl+Chow (grey, n = 10), Ctrl+HFD (black, n = 10), DT+Chow (pink, n = 8), DT + HFD (red, n = 11) over 24 weeks of HFD. Right panel: AUC. P-values: Ctrl+chow vs Ctrl+HFD P < 0.62, Ctrl+chow vs DT+chow P = 0.12, Ctrl+chow vs DT + HFD P = 0.13, Ctrl+HFD vs DT+chow P = 0.03, Ctrl+HFD vs DT + HFD P = 0.04; DT+chow vs DT + HFD P = 0.97. **c**, Intraperitoneal glucose tolerance test (ipGTT) 24-weeks after HFD of Ctrl+chow (grey, n = 10), Ctrl+HFD (black, n = 10), DT+chow (pink, n = 8), DT + HFD (red, n = 11). Right panel: AUC. P-values: Ctrl+chow vs Ctrl+HFD P = 0.0073, Ctrl+chow vs DT+chow P = 0.0.0038, Ctrl+chow vs DT + HFD P = 0.9404, Ctrl+HFD vs DT+chow P < 0.0001, Ctrl+HFD vs DT + HFD P = 0.0012; DT+chow vs DT + HFD P = 0.0129. **d**, Plasma insulin release at 0 and 15 minutes after glucose injection in Ctrl+chow (grey, n = 9), Ctrl+HFD (black, n = 10), DT+chow (pink, n = 8), DT + HFD (red, n = 11). P-values: Ctrl+Chow (0′vs15′) P = 0.0039; Ctrl+HFD (0′vs15′) P = 0.0355; DT+Chow (0′vs15′) P = 0.0281; DT + HFD (0′vs15′) P = 0.0192. Ctrl+HFD vs DT + HFD at 0′ P = 0.0357; Ctrl+HFD vs DT+Chow at 15′ P = 0.0044; Ctrl+HFD vs DT + HFD at 15′ P = 0.0101. Only male mice were used. All data are shown as mean ± sem. All statistical tests are two-tailed Mann-Whitney test. Source data is available.

https://doi.org/10.1038/s42255-024-01114-8

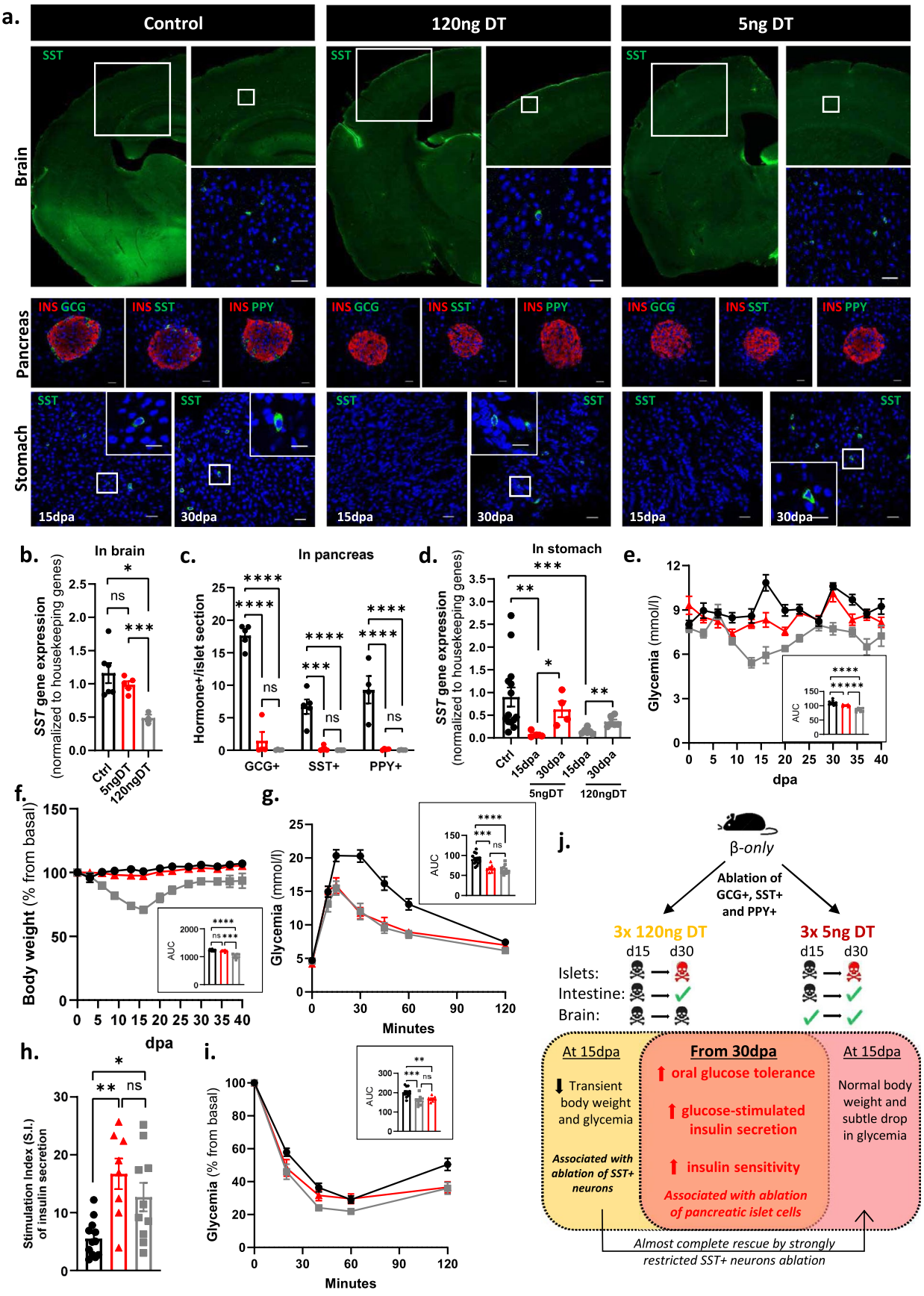

Extended Data Fig. 7 | See next page for caption.

https://doi.org/10.1038/s42255-024-01114-8

Extended Data Fig. 7 | Improved glucose homeostasis after the specific ablation of the pancreatic α-, δ-, and γ-cells. a. Immunofluorescence from control (Ctrl, left panel), mice injected with 120 ng of DT (middle panel) or 5 ng of DT (right panel). Top row: Brain somatostatin (green). Mid row: islet insulin (red), glucagon, somatostatin or Ppy (green). Bottom row: stomach somatostatin (green). Scale bars: 20 µm or 10 µm (insets). **b**. Brain qPCR on SST in Ctrl (black; n = 6) and 120ngDT (grey; n = 3) or 5ngDT (red; n = 5). Data are normalized ct values relative to β-actin and Gapdh. P-values: Ctrlvs5ngDT P = 0.6623, Ctrlvs120ngDT P = 0.0238, 5ngDTvs120ngDT P = 0.0357. **c**. Quantification of pancreatic GCG+, SST+, and PPY+ cells in Ctrl (black; n = 5), 120ngDT (grey; n = 4) or 5ngDT (red; n = 4). P-values: GCG+ Ctrlvs5ngDT P < 0.0001, Ctrlvs120ngDT P < 0.0001, 5ngDTvs120ngDT P = 0.5783. SST+ Ctrlvs5ngDT P = 0.0001, Ctrlvs120ngDT P < 0.0001, 5ngDTvs120ngDT P = 0.9852. PPY+ Ctrlvs5ngDT P < 0.0001, Ctrlvs120ngDT P < 0.0001, 5ngDTvs120ngDT P = 0.9964. **d**. Stomach qPCR on SST in Ctrl (black; n = 14) and 120ngDT (grey; n = 4) or 5ngDT (red; n = 4). Data are normalized ct values relative to β-actin and Gapdh. P-values: Ctrlvs5ngDT at 15 dpa P = 0.0013; Ctrlvs5ngDT at 30 dpa P = 0.7209; Ctrlvs120ngDT at 15 dpa P = 0.0006; Ctrlvs120ngDT at 30 dpa P = 0.0676; 5ngDT 15dpavs30dpa P = 0.0286; 120ngDT 15dpavs30dpa P = 0.0043. **e-f**. Glycemia (e) and body weight (f, % of change) of Ctrl (black; n = 12), 120ngDT (grey; n = 7) or 5ngDT (red; n = 8). Small panel: area under the curve (AUC). P-values: Glycemia Ctrlvs5ngDT P = 0.0017; Ctrlvs120ngDT P < 0.0001; 5ngDTvs120ngDT P = 0.003. Body weight Ctrlvs5ngDT P = 0.1196; Ctrlvs120ngDT P < 0.0001; 5ngDTvs120ngDT P = 0.003. **g**. Oral glucose tolerance test (oGTT) in Ctrl (black; n = 14), 120ngDT (grey; n = 10) or 5ngDT (red; n = 8). P-values: Ctrlvs5ngDT P = 0.0003; Ctrlvs120ngDT P < 0.0001; 5ngDTvs120ngDT P = 0.4215. **h**. Stimulation index (S.I.) of insulin in Ctrl (black; n = 12), 120ngDT (grey; n = 10) or 5ngDT (red; n = 8). P-values Ctrlvs5ngDT P = 0.0011; Ctrlvs120ngDT P = 0.0206; 5ngDTvs120ngDT P = 0.2844. **i**. Insulin tolerance test (ITT) in Ctrl (black; n = 14), 120ngDT (grey; n = 9) or 5ngDT (red; n = 8). Data are shown as % relative to glycemia at time 0. Right panel: AUC. P-values Ctrlvs5ngDT P = 0.0072; Ctrlvs120ngDT P = 0.0005; 5ngDTvs120ngDT P = 0.7979. **j**. Graphical summary. Only male mice were used. Error bars denote s.e.m. Two-way ANOVA and two-tailed Mann-Whitney test are used. Source data is available.

https://doi.org/10.1038/s42255-024-01114-8

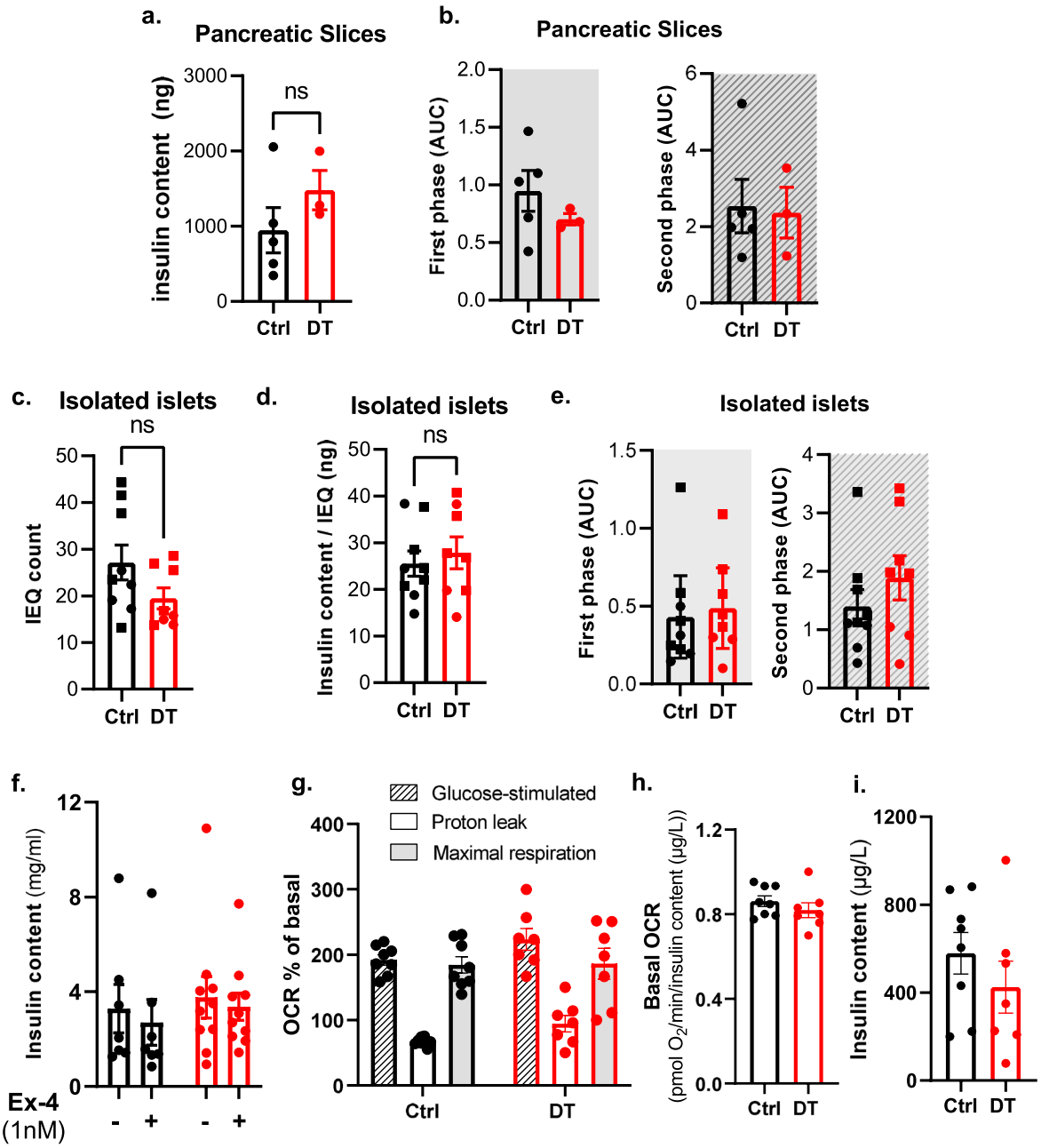

Extended Data Fig. 8 | Ex vivo dynamic insulin secretion in pancreatic slices and isolated islets. a, Pancreatic insulin content (ng) of slices from control (Ctrl, black, n = 5) and DT (red, n = 3). P-value CtrlvsDT=0.250. **b**, Area under the curve (AUC) of the first phase (grey area, 14- and 24-minutes) and second phase (dashed grey area, 30- and 58-minutes). P-values (CtrlvsDT): first phase P = 0.393; second phase P = > 0.999. **c-d**, Islet equivalent count (IEQ, c) and ratio insulin content (ng) and IEQ count (d) of Ctrl (black, n = 9) and DT (red, n = 8). P-value: IEQ count (CtrlvsDT) P = 0.2359; ratio insulin content and IEQ (CtrlvsDT) P = 0.743. **e**, AUC of first phase (P-value CtrlvsDT P = 0.393) and second phase (P-value CtrlvsDT P = > 0.999) of insulin secretion in isolated islets of Ctrl (black; n = 9) and DT (red; n = 8) mice. **f**, Total insulin content (ng) of isolated islets from Ctrl (black, n = 7) and DT (red, n = 10) mice with or without Exendin-4 (Ex-4). P-value without Ex-4 CtrlvsDT P = 0.601; P-value with Ex-4 CtrlvsDT P = 0.3031. g-h. Islet respirometry parameters. **g**. Glucose-stimulated OCR (dashed lined column), proton leak and maximal respiration (grey column) in islets from Ctrl (black, n = 8) and DT (red, n = 7) mice. P-values (CtrlvsDT): Glucose-stimulated OCR P = 0.3285; Proton leak P = 0.2046; Maximal respiration P = 0.999. **h**. Basal respiration measured at 3 mM glucose from Ctrl (black, n = 8) and DT (red, n = 7). 2-4 wells/mice, 8-10 islets/well. P-values Ctrl vs DT P = 0.281. **i**. Total insulin content of islets from Ctrl (black, n = 8) and DT (red, n = 7) after OCR measurements. P-values CtrlvsDT P = 0.3357. Each data point (g-i) represents the average values per mouse. Only male mice were used. All data are shown as mean ± sem. All statistical tests are two-tailed Mann-Whitney test. Source data is available.

https://doi.org/10.1038/s42255-024-01114-8

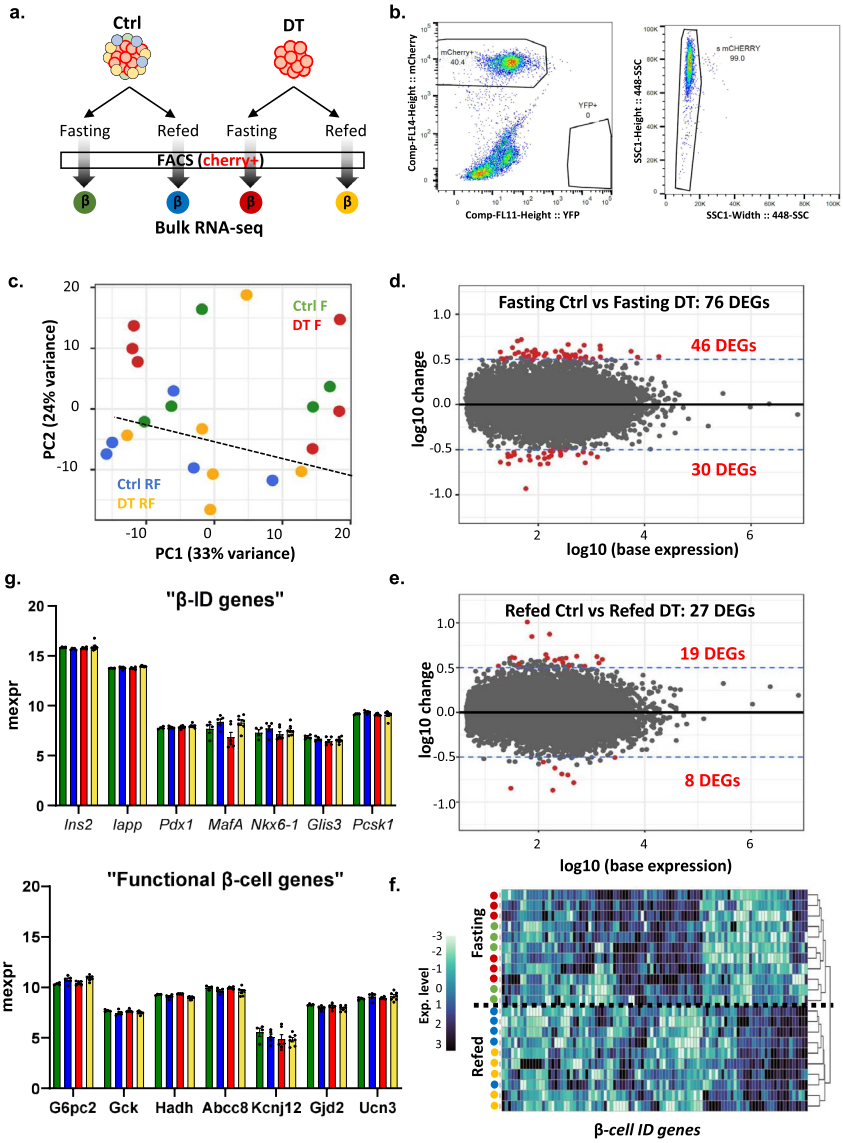

Extended Data Fig. 9 | Transcriptomic analysis of β-cells isolated from control and β-only mice. a, Experimental design. **b**, Representative gating strategy used for FACS sorting the mCherry+ insulin-expressing cells in Ctrl and β-only mice for RNA-seq analysis. **c**, Principal component analysis (PCA) of RNA-seq samples. Each dot represents one sample. Four different conditions: Control Fasting (Ctrl F, green, n = 5), DT Fasting (DT F, red, n = 6), Control Refed (Ctrl RF, blue, n = 5) and DT Refed (DT RF, yellow, n = 6). **d-e**, MA plot of the DEGs (differentially expressed genes) between DT and Ctrl during 8-hour fasting (d) and after 2-hour refeeding (e). Each dot represents one gene. Red dots are the genes with p-values < 0.05 and a log fold change >0.5 or <−0.5. **f**, Heatmap showing scaled expression (blue, high expression; white, low expression) of representative β-ID genes. The dendrogram represents the clustering of each condition analyzed based on β-ID genes expression. **g**, Expression levels of key identity (top panel) and functional (bottom panel) β-cell genes during fasting in controls and DT-treated mice after 8-hour fasting or 2-refeeding. P-values for all genes and conditions are non significant (P > 0.05). Only male mice were used. Data are shown as mean ± sd. All statistical tests are two-tailed Mann-Whitney test. Source data is available.

https://doi.org/10.1038/s42255-024-01114-8

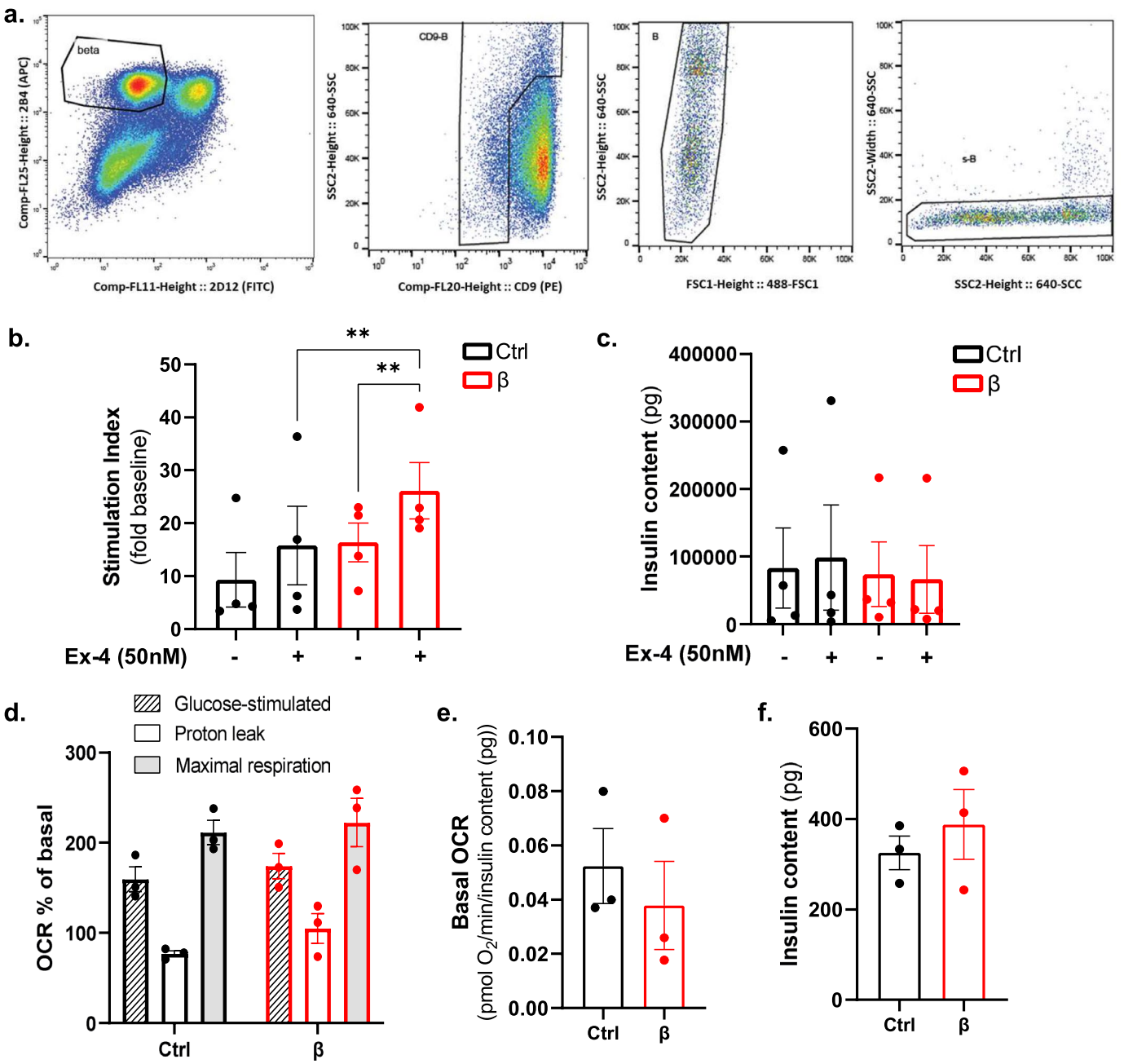

Extended Data Fig. 10 | Stimulatory index and glucose-stimulated oxygen consumption are maintained in human monotypic β-pseudoislets. a. FACS strategy used to purify human β-cells. Representative plots of cells labelled with the pan-endocrine marker HIC1-2B4, the non-β-cell endocrine marker H1C3-2D12 and the δ-cell enriched marker CD9. **b**. Stimulation index of absolute insulin secretion at 16.7 mM glucose in presence/absence of the GLP-1 agonist Exendin-4 (Ex-4, 50 nM) in pseudoislets composed by all cell types (Ctrl, black) and only β-cells (red). Values are expressed as fold change to baseline values measured at 3 mM glucose (low glucose, LG). N = 4 donors. **c**. Total insulin content of control (black) and β-only pseudoislets (red) measured after stimulation at 16.7 mM glucose (high glucose, HG). N = 4 donors. P-values (Ctrl vs β): HG P = 0.9708, HG+Ex4 P = 0.4343. P-values Ctrl HG vs HG+Ex4 P = 0.8848. P-values β HG vs HG+Ex4 P = 0.9843. d-f. Pseudoislet respirometry parameters from Fig. 6e. N = 3 independent donors. 2-5 wells/condition/donor, 10 pseudoislets/well. Each data point represents the well average per donor. **d**. Glucose-stimulated OCR (dashed lined column), proton leak and maximal respiration (grey column) in control (black) and monotypic β-pseudoislets. P-values (Ctrl vs β): Glucose-stimulated OCR P = 0.872; Proton leak P = 0.539; Maximal respiration P = 0.982. (red). **e**. Basal respiration measured at 3 mM glucose before injections. P-values Ctrl vs β P = 0.4. **f**. Total insulin content of control (Ctrl) and β-pseudoislets (red) after OCR measurements. P-values Ctrl vs β P = 0.7. Both male and female human donors were used. All data are shown as mean ± sem. All statistical tests are two-tailed Mann-Whitney test. Source data is available.

nature portfolio

Corresponding author(s): Pedro Luis Herrera

Last updated by author(s): Jul 8, 2024

Reporting Summary

Nature Portfolio wishes to improve the reproducibility of the work that we publish. This form provides structure for consistency and transparency in reporting. For further information on Nature Portfolio policies, see our Editorial Policies and the Editorial Policy Checklist.

Statistics

For all statistical analyses, confirm that the following items are present in the figure legend, table legend, main text, or Methods section.

n/a	Confirmed	
☐	☒	The exact sample size (*n*) for each experimental group/condition, given as a discrete number and unit of measurement
☐	☒	A statement on whether measurements were taken from distinct samples or whether the same sample was measured repeatedly
☐	☒	The statistical test(s) used AND whether they are one- or two-sided *Only common tests should be described solely by name; describe more complex techniques in the Methods section.*
☒	☐	A description of all covariates tested
☒	☐	A description of any assumptions or corrections, such as tests of normality and adjustment for multiple comparisons
☐	☒	A full description of the statistical parameters including central tendency (e.g. means) or other basic estimates (e.g. regression coefficient) AND variation (e.g. standard deviation) or associated estimates of uncertainty (e.g. confidence intervals)
☐	☒	For null hypothesis testing, the test statistic (e.g. *F*, *t*, *r*) with confidence intervals, effect sizes, degrees of freedom and *P* value noted *Give P values as exact values whenever suitable.*
☒	☐	For Bayesian analysis, information on the choice of priors and Markov chain Monte Carlo settings
☒	☐	For hierarchical and complex designs, identification of the appropriate level for tests and full reporting of outcomes
☒	☐	Estimates of effect sizes (e.g. Cohen's *d*, Pearson's *r*), indicating how they were calculated

Our web collection on statistics for biologists contains articles on many of the points above.

Software and code

Policy information about availability of computer code

Data collection	Moflo Astrios (Beckman Coutler) system on Summit v6.2 (Beckman Coutler) software. Seahorse XFe96 system on Seahorse Wave Controller Software 2.6 (Agilent) Data collection was mainly performed using Microsoft Excel.
Data analysis	Analysis of the FAC-sorting data was done on Kaluza Analysis v 2.0 (Beckman Coulter) software. Analysis of islet respirometry was done on Wave Software 2.6.1 (Agilent). For bluk RNA-seq, reverse transcription and cDNA amplification were performed using the SMARTer Ultra Low RNA kit (Clontech). cDNA libraries were prepared using Nextera XT DNA Sample Preparation kit (Illumina) and sequenced on an Illumina HiSeq4000 platform with single-end 100-bp. All sequencing data were uploaded to and aligned on the Galaxy project (PMID: 27137889) against Ensembl reference genome GRCm38.p6 (release 100) using STAR version 2.7.2b (PMID: 23104886) n 2-pass mapping mode. Aligned data were counted using HTSeq version 0.9.1 (PMID: 25260700) in union mode. Analyses were performed in a pair-wise manner between the four conditions analyzed using DESeq2 version 1.28.1 (PMID: 25516281). For each pairwise comparison, genes were discarded if they had fewer than 5 counts per sample on average. After calculating differential expression between groups, log2 fold changes were shrunken using the normal estimator (PMID: 25516281). Genes were considered to be differentially expressed if the absolute shrunken log2 fold changes were equal to or above 1, and adjusted p-values were equal to or below 0.05. Normalization and analysis of the qPCR data were done with the RT-PCR analysis_macro v1.1 (from the Genomic Platform, University of Geneva) using two normalization genes (Gapdh and β-actin).

In all experiments cells were manually counted and considered positive for a marker when one nucleus was clearly surrounded by the hormone.

Data analysis was performed using Microsoft Excel.

All statistical analyses were performed with GraphPad Prism v9.0.

For manuscripts utilizing custom algorithms or software that are central to the research but not yet described in published literature, software must be made available to editors and reviewers. We strongly encourage code deposition in a community repository (e.g. GitHub). See the Nature Portfolio guidelines for submitting code & software for further information.

Data

Policy information about availability of data

All manuscripts must include a data availability statement. This statement should provide the following information, where applicable:

- Accession codes, unique identifiers, or web links for publicly available datasets
- A description of any restrictions on data availability
- For clinical datasets or third party data, please ensure that the statement adheres to our policy

The mouse β-cell bulk RNA-seq generated in this study have been deposited in the NCBI GEO database with the accession number GSE226479 (https://www.ncbi.nlm.nih.gov/geo/query/acc.cgi?acc=GSE226479). All sequencing data were uploaded to and aligned on the Galaxy project80 against Ensembl reference genome GRCm38.p6 (release 100) (https://www.ensembl.org/Mus_musculus/Info/Index). The unfiltered list of differentially expressed genes is provided as Supplementary Information. The β-ID gene list generated by van Gurp et al. 2022 (NCBI GEO database with the accession number: GSE150724) was used for analysis.

Source data for Figs. 1-6 and Extended Data Figures are provided with this paper in Source Data files, availability of associated source data is indicated in each figure legend.
Donor details for human samples are available in Extended Data Supplementary Table 4.

All data and materials used are available from the authors or from commercially available sources. This data is available in the Methods section.

Research involving human participants, their data, or biological material

Policy information about studies with human participants or human data. See also policy information about sex, gender (identity/presentation), and sexual orientation and race, ethnicity and racism.

Reporting on sex and gender	We did not discriminate in sex/gender for human islet experiments. All information about human donors are described in Extended Data Table 4.
Reporting on race, ethnicity, or other socially relevant groupings	All information about human donors are described in Extended Data Table 4.
Population characteristics	All information about human donors are described in Extended Data Table 4.
Recruitment	We did not recruit human participants. All human islet samples are isolated from cadaveric donors at isolation centers.
Ethics oversight	All studies involving human samples were approved by ethical committee in University of Geneva.

Note that full information on the approval of the study protocol must also be provided in the manuscript.

Field-specific reporting

Please select the one below that is the best fit for your research. If you are not sure, read the appropriate sections before making your selection.

☒ Life sciences ☐ Behavioural & social sciences ☐ Ecological, evolutionary & environmental sciences

For a reference copy of the document with all sections, see nature.com/documents/nr-reporting-summary-flat.pdf

Life sciences study design

All studies must disclose on these points even when the disclosure is negative.

Sample size	Sample size was chosen to ensure adequate power and to detect a pre-specified effect based on the available literature and protocols in the field. Therefore, sample sizes are comparable with the ones used in the published literature in the field. For multiple transgenics and human samples the numbers were also limited by the availability of the phenotype. No statistical methods were used to predetermine sample size.
Data exclusions	At the beginning of each experiment, mice must be (1) healthy, (2) normoglycemic, (4) bearing all the desired transgenes, (5) for age-matched controls we prefered, when possible, litter mates. These exclusion criteria were pre-established.

Replication	All experiments were performed independently and replicated at least once; except for the human experiments, which could only be performed once due to restricted number of material. All attempts at replication were successful.
Randomization	In all mouse experiments, we randomly selected in each litter the experimental and control animals. Co-variates such as the health status of the mice over the experimental design were considered for the data analysis. Mice were weekly controlled for body weight and glycemia. In the experiments using human donor samples, sample selections were not randomized. Only non-diabetic human donors were selected.
Blinding	Most of the experiments were performed blind. For some experiments (such as S961 treatment), blinding was not possible due to regular control of the hyperglycemia in the treated animals. In vitro experiments, investigators were blinded to group allocation during data collection and analysis.

Reporting for specific materials, systems and methods

We require information from authors about some types of materials, experimental systems and methods used in many studies. Here, indicate whether each material, system or method listed is relevant to your study. If you are not sure if a list item applies to your research, read the appropriate section before selecting a response.

Materials & experimental systems

n/a	Involved in the study
☐	☒ Antibodies
☒	☐ Eukaryotic cell lines
☒	☐ Palaeontology and archaeology
☐	☒ Animals and other organisms
☒	☐ Clinical data
☒	☐ Dual use research of concern
☒	☐ Plants

Methods

n/a	Involved in the study
☒	☐ ChIP-seq
☐	☒ Flow cytometry
☒	☐ MRI-based neuroimaging

Antibodies

Antibodies used	The primary antibodies used were: guinea pig anti-insulin (1/400; DAKO, A0564), rabbit anti-insulin (1/3000; Molecular Probes, 701265), chicken anti-insulin (1:200; Abcam ab14042); rabbit anti-insulin (1:300, Cell signaling, 3014), mouse anti-glucagon (1/1000; Sigma, G2654), rabbit anti-glucagon (1/200; DAKO, A0565), mouse anti-somatostatin (1/200; BCBC Ab1985), rabbit anti-somatostatin (1/200; DAKO, A0566), rat anti-somatostatin (1:200; Merck Mab354), mouse anti-Ppy (1/400; Santa Cruz, MAB62971), goat anti-Ppy (1/300; Novus Biologicals, NB 100-1793), goat anti-Glp1 (1:100; Santa Cruz sc-7782), rabbit andti-Ki67 (1:700, Epredia, RM-9106). Sections were also stained with DAPI. Secondary antibodies were coupled to Alexa fluorophores. Goat anti-rabbit Alexa 488 (1/500; Molecular Probes; 1070-03), donkey anti-goat Alexa 568 1/500; Molecular Probes; A-11057), goat anti-guinea pig Alexa 647 (1/500; Molecular Probes; A-21450). Goat anti-mouse TRITC (1/500; Southern Biotech, 1070-03) was also used.
Validation	All antibodies used were validated by the respective commercial source for the application used in this manuscript.

Animals and other research organisms

Policy information about studies involving animals; ARRIVE guidelines recommended for reporting animal research, and Sex and Gender in Research

Laboratory animals	Sst-DTR mice were generated under a C57BL/6 background. Then, these Sst-DTR mice were crossed with Gcg-DTR and Ppy-DTR mice, with a mix background. All transgenic mice (non-beta-DTR mice) used in this study had a mixed background. 2-3 months old male and female mice were used for all experiments. Except for long-term following of alpha, delta and gamma-cell ablated animals, which were kept until one-year-old.
Wild animals	No wild animals were used in this study.
Reporting on sex	Most of the experiments were performed on male mice for simplicity in interpreting the results. However, females were also used to confirm the main phenotype observed in the study.
Field-collected samples	No field-collected samples were used in this study.
Ethics oversight	The study follows all ethical regulations regarding animal experimentation, all experiments were performed under the guidelines of the Direction General de la Santé du Canton de Genève (license numbers: GE/111/17, GE/121/17 and GE15820).

Note that full information on the approval of the study protocol must also be provided in the manuscript.

Plants

Seed stocks

Report on the source of all seed stocks or other plant material used. If applicable, state the seed stock centre and catalogue number. If plant specimens were collected from the field, describe the collection location, date and sampling procedures.

Novel plant genotypes

Describe the methods by which all novel plant genotypes were produced. This includes those generated by transgenic approaches, gene editing, chemical/radiation-based mutagenesis and hybridization. For transgenic lines, describe the transformation method, the number of independent lines analyzed and the generation upon which experiments were performed. For gene-edited lines, describe the editor used, the endogenous sequence targeted for editing, the targeting guide RNA sequence (if applicable) and how the editor was applied.

Authentication

Describe any authentication procedures for each seed stock used or novel genotype generated. Describe any experiments used to assess the effect of a mutation and, where applicable, how potential secondary effects (e.g. second site T-DNA insertions, mosiacism, off-target gene editing) were examined.

Flow Cytometry

Plots

Confirm that:

☒ The axis labels state the marker and fluorochrome used (e.g. CD4-FITC).

☒ The axis scales are clearly visible. Include numbers along axes only for bottom left plot of group (a 'group' is an analysis of identical markers).

☒ All plots are contour plots with outliers or pseudocolor plots.

☒ A numerical value for number of cells or percentage (with statistics) is provided.

Methodology

Sample preparation

Mouse RNA-Seq analyses. Islet cells were obtained from one month after DT treatment of Glucagon-DTR; Somatostatin-DTR; Ppy-DTR mice. Islet isolation and cell isolation by flow cytometry (FACS) were performed using previously described protocols (Chera et al 2014).

Human islet cell sorting. Samples were obtained from isolated islets from cadaveric donors at isolation centers. Samples were prepared using previously described protocols (Furuyama et al 2019)

Instrument

Cell sorting using FACS were performed using a Moflo Astrios (Beckman Coutler) system.

Software

Cell sorting was performed on Summit v 6.2 (Beckman Coulter) software. Kaluza Analysis v 2.0 (Beckman Coulter) software was used for subsequent analysis.

Cell population abundance

For mouse experiments. For validation of the purity, small fractions of sorted cells were FACS-sorted again to confirm the gating strategy.

For human experiments. For evaluation of cell purity, sorted islet cell fractions were immunostained for insulin, glucagon, somatostatin and pancreatic polypeptide. Stained cells were examined with a confocal microscope (Leica TCS SPE). Confirmation of the purity of beta-pseudoislets was performed for each donor by immunostaining and qPCR for each hormone. Only batches with high purity (> 98%) were used in following experiments.

Gating strategy

Single viable islet cells were gated by forward scatter, side scatter and pulse-width parameters and by negative staining for DAPI (Life Technologies) or DRAQ7 (B25595, BD Biosciences) to remove doublets and dead cells.
In mice experiments, boundaries between positive and negative were very clear because of very high expression of reporter proteins.
In human experiments, beta-cell population was gated on HIC1-2B4 and HIC3-2D12. The fraction was further purified based on CD9 and FSC/SSC.

☒ Tick this box to confirm that a figure exemplifying the gating strategy is provided in the Supplementary Information.